1 2 9 0

UNIVERSIDADE Ð
COIMBRA

Kapil Kumar Shrestha

RELATIONSHIP BETWEEN THE FRICTION COEFFICIENT AND THE MICROSTRUCTURE CHANGES OCCURRING IN SLIDING CONTACT WITH CROSSED CYLINDERS

VOLUME 1

July 2021

Relationship between the friction coefficient and the microstructure changes occurring in sliding contact with crossed cylinders

Submitted in Partial Fulfilment of the Requirements for the Degree of European Joint European Master in Tribology of Surfaces and Interfaces.

Author

Kapil Kumar Shrestha

Advisor

Doutor Carlos Wagner Moura e Silva

Professor Doutor Albano Cavaleiro

Jury

President	**Professor Doutor Bruno Trindade** **Professor at University of Coimbra**
Vowel	**Doutor Ricardo Serra** **Investigator at University of Coimbra**
Advisor	**Professor Doutor Albano Cavaleiro** **Professor at University of Coimbra**

UNIVERSIDADE DE COIMBRA

tribos

Joint European Master in Tribology of Surfaces and Interfaces

Ljubljana • Leeds • Coimbra • Luleå

Coimbra, July 2021

Acknowledgments

First of all, I would like to express my deepest gratitude to my Master Thesis advisors, Dr. Carlos Wagner Moura e Silva and Prof. Dr. Albano Cavaleiro from the University of Coimbra, for their guidance and valuable input during the course of the project. I would like to thank Dr. Manuel Evaristo and Dr. Todor Vuchkov, who helped deposit the coatings. Also, to Carlos Patacas of IPN for all the technical contributions for this work.

Special thanks to the TRIBOS consortium for this life-changing opportunity and the European Commission for the funding provided.

Finally, I want to acknowledge my parents, families, and friends who have offered continuous support and encouragement, directly or indirectly, throughout my time in this master's program.

Abstract

Several studies have been done until now to replicate the contact conditions between the tool and the workpiece. This research has been limited to hard-coated tools, although the advantages of self-lubricating coated tools for cutting and forming operations can be even superior. The present study aims to establish the relationship between the coefficient of friction and the microstructure change in coated samples in a modified crossed cylinder test. For the study, self-lubricating coatings such as WSC, DLC-W, DLC-Si(O), and DLC were evaluated. The chemical composition and morphology of the coatings were investigated using SEM/WDS, whereas hardness was evaluated by nanoindentation testing. A modified crossed cylinder test was used at room temperature and dry conditions to understand the tribological behavior of self-lubricating coatings that mimic the real contact of metal forming operation. Finally, wear areas were investigated under an optical microscope and SEM/EDS. Raman spectroscopy was also used to confirm some of the results. It is concluded that the coefficient of friction decreases with the increase of load for all coatings except DLC-Si(O), and the hardness is one of the major parameters responsible for the wear rate. The low-friction behavior of WSC could be related to the formation of a low friction tribolayer on its sliding surface. Also, the presence of additional elements in the structure of the DLC coating can cause a reduction in the internal stresses of the coating without compromising its tribological performance.

Keywords: Self-lubricating coatings, Modified crossed cylinder test, Coefficient of friction, Microstructure changes.

Resumo

Vários têm sido os estudos para replicar as condições de contacto entre um ferramenta e a peça a produzir. Este estudo foi limitado a ferramentas revestidas com filmes duros, embora as vantagens das mesmas revestidas com filmes auto-lubrificantes, para operações de corte e de enformação, possam mesmo ser superiores. Pretendeu-se estabelecer a relação entre o coeficiente de atrito e a alteração da microestrutura em amostras revestidas usando para isso um teste de cilindros cruzados. Para este estudo, foram analisados revestimentos auto-lubrificantes, tais como WSC, DLC-W, DLC-Si(O) e DLC. Foram avaliadas a composição química e a morfologia dos revestimentos, utilizando SEM/WDS, enquanto que a dureza foi medida por nanoindentação. O comportamento trifológico de revestimentos auto-lubrificantes foi avaliado à temperatura ambiente e em condições de não-lubrificação no teste de cilindros cruzados, pretendendo-se imitar o contacto real das operações de enformação de metais. Finalmente, as pistas de desgaste foram analisadas por microscopias ótica e eletrónica de varrimento (SEM/EDS). A espectroscopia de Raman permitiu confirmar alguns dos resultados estruturais. Conclui-se que o coeficiente de atrito diminui com o aumento da carga para todos os revestimentos, com exceção da DLC-Si(O), e que a dureza é um dos principais parâmetros responsáveis pelo coeficiente de desgaste. O comportamento de baixa atrito do WSC pode estar relacionado com a formação de tribo camadas de baixo atrito na superfície deslizante. Além disso, a presença de elementos adicionais na estrutura do revestimento DLC pode causar uma redução das tensões internas do revestimento sem comprometer o seu desempenho trilógico.

Palavras-chave: Revestimentos auto-lubrificantes, Teste de cilindros cruzados modificado, Coeficiente de atrito, Alterações de microestrutura.

Table of Contents

List of abbreviations

Abbreviation	Meaning
CVD	Chemical vapor deposition
PVD	Physical vapor deposition
ASTM	American Society for Testing and Materials
ISO	International Organization for Standardization
W-S-C	Tungsten-sulfur-carbon
WDS	Wavelength dispersive spectroscopy
TMD	Transition Metal Dichalcogenides
SEM	Scanning electron microscope
XRD	X-Ray Diffraction
DLC	Diamond-like carbon
HCF	High cycle fatigue
LCF	Low cycle fatigue
RT	Room temperature
HSS	High speed steel
COF	Coefficient of friction
EDS	electron dispersive spectroscopy
XPS	X-ray photoelectron spectroscopy
HiPIMS	High power impulse magnetron sputtering
DC	Direct Current
IPN	Institute Pedro Nunes
λ_m	Effective mean wear rate

List of figures

List of tables

1. Introduction

A crucial challenge for modern technology is sustainable development and the ways to manage with the limited resources of material and energy. So, finding new technology to produce it; is as important as limiting the resource available. Tribology, the branch of science which deals with the concept of friction and wear, relates the fundamentals of energy and material loss. Much energy is lost to overcome friction in various systems. Therefore, reducing friction and wear provides the opportunity to save energy and material, prolonging mechanical components' life.

One solution to prevent wear and minimize friction is to use lubricants, which prevent two surfaces from making close contact. In the case of liquid lubrication, the contact temperature can also be reduced. However, in many cases, the use of lubricants is neither possible nor recommended, many times to prevent contamination between the sliding objects. Therefore, the design and development of self-lubricating coatings are becoming a huge area of interest.

Self-lubricating coatings have been used in metal forming tools to prolong the tool life and reduce the coefficient of friction. Different techniques such as thermal spraying, chemical vapor deposition (CVD), physical vapor deposition (PVD), electrochemical and electroless processes, or thermochemical processes, are used to produce hard, wear-resistant, and low friction coatings. The description of numerous coating deposition techniques is available in the literature (see, e.g. [1]). The application of engineered surface coatings to increase the wear resistance of components and parts requires knowledge of their tribological behavior, which can be achieved through wear tests. These tests are selected and used to optimize the coating development for a specific application [2].

This work focuses on studying the relation between the coefficient of friction and the microstructure changes occurring in crossed cylinder wear testing. This wear test has been used a long time ago by Sato et al. [3] and, more recently, by Zhu et al. [4], Gerth et al. [5], and Heinrichs et al. [6].

2. Framework

The research project presented in this work is being performed to fulfill the requirement of the completion of the Joint European Masters in Tribology of Surfaces and Interfaces. The title of the project is "Relationship between the friction coefficient and the microstructure changes occurring in sliding contact with crossed cylinders." It is carried out at the premises of CEMMPRE, the Center for Mechanical Engineering, Materials and Processes of the University of Coimbra.

This work's primary focus and goal are to evaluate the relationship between the friction coefficient and the microstructural modification resulting from the application of a constant force through a sliding contact technique with crossed cylinders without lubrication. A brief description of the current work and its findings related to this project will be presented in the following section. Also, the detailed information on the methodology to follow, the selected materials (work samples and coatings) to be used, and the necessary equipment are explained in separate headings. Finally, the timeline of this project will be outlined at the end of this text.

3. State of the Art

3.1 Friction in tribology

Tribology is the science of interacting surfaces which are moving relative to each other. Generally, the subjects, friction, wear, and lubrication, are studied and are related to many aspects of our daily life. Minimizing the friction and wear results in lower energy consumption which is now a priority for a sustainable world.

Friction is the force that generates when two objects that are in contact moving with some relative velocity. Four types of friction generated from different sliding contact forms can be considered: sliding, static, fluid, and rolling. The sliding, static, and rolling friction are related to solids surfaces, while fluid friction occurs in liquids and gasses.

Static friction is generated when a body starts to slide on a static surface [7]. We can walk on roads due to static friction; without this friction, we cannot move forward, and our shoes would slide on the pavement. Another example of static friction is when we hammer the nail in the wood; the nail stay is due to static friction.

Sliding friction is an addiction that acts on an object moving on another surface with some relative velocity shown by the schematic picture in fig 1. This friction is generated after eliminating the static friction when an object moves from the rest position to a certain velocity. The pencil (lead) when slides on the paper, the generated friction leaves a mark on the paper. The sliding friction is usually smaller than the static friction between the two objects having the same roughness factor.
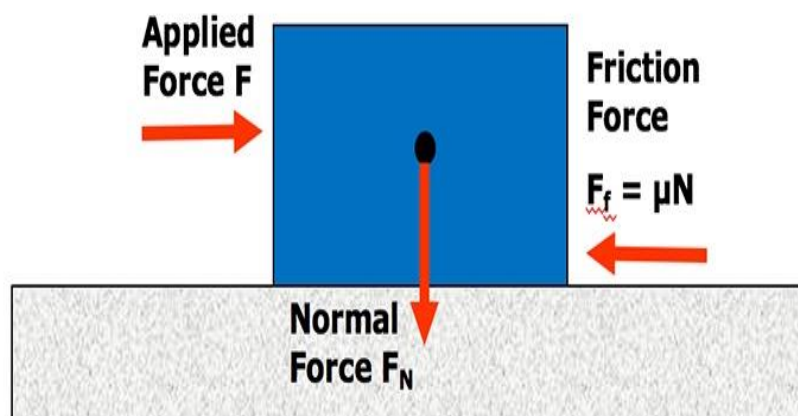
Figure 1 Schematic picture showing the normal (F_N) and friction (F_F) forces on sliding [8]

The magnitude of the sliding friction is dependent on various factors [9] as described below:

- The smoothness/roughness of the surfaces in contact
- The speed of either object
- The surface contact area
- The pressure on either object
- The adhesion between the two surfaces

Mathematically the sliding friction is equal to the friction coefficient times the normal force.

$$F_k = \mu_k * F_n$$

Where F_k = sliding friction force

μ_k = sliding friction coefficient

F_n = normal force

The frictional force at rest or zero sliding velocity is the static friction. The magnitude of frictional force at different velocities was studied by Lee et al. [10]. They observed that frictional force at rest is higher than coulomb frictional force at nonzero velocity, as shown in Fig. 2 due to the coefficient of static friction (μ_s) being larger than the coefficient of kinetic friction (μ_k).
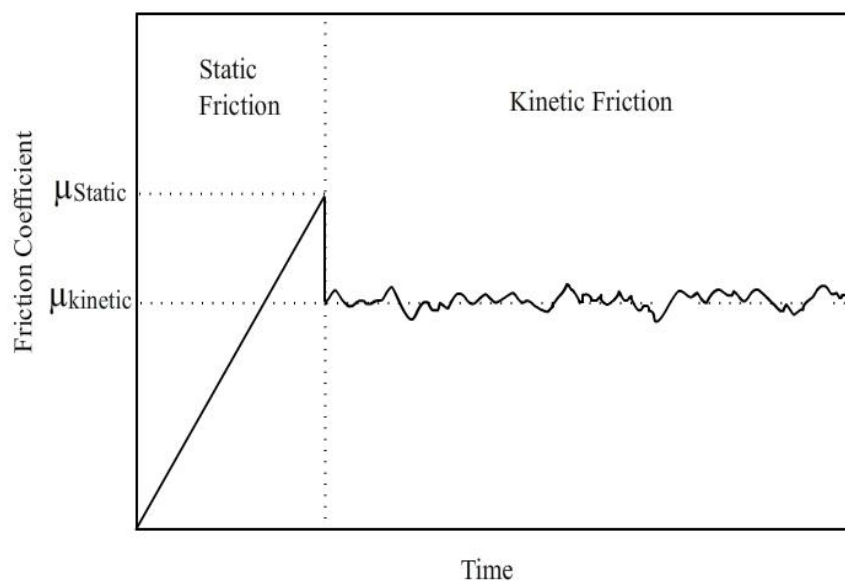
Figure 2 Static and kinetic friction [10]

3.2 Types of wear and wear mechanism

Wear is defined as a progressive loss of a substance that is in contact due to mechanical action. Generally, these substances are in relative motion rolling, sliding, or under load. The wear occurs due to the mechanical failure of a highly stressed surface. There are three mechanisms of wear that are referred to as abrasive wear, adhesive wear, and fatigue wear.

3.2.1 Abrasive Wear

Abrasive wear is usually due to small particles embedded either on the surface of one of the elements of the sliding pair or between the sliding surfaces. ASTM G174 is the standard test to measure the abrasive resistance of different materials by using an abrasive loop contact. The abrasive resistance is usually classified by the contact type and the contact environment. There are two types of modes for abrasive wear: the two-body and the three-body contact [11], as shown in the figure below.
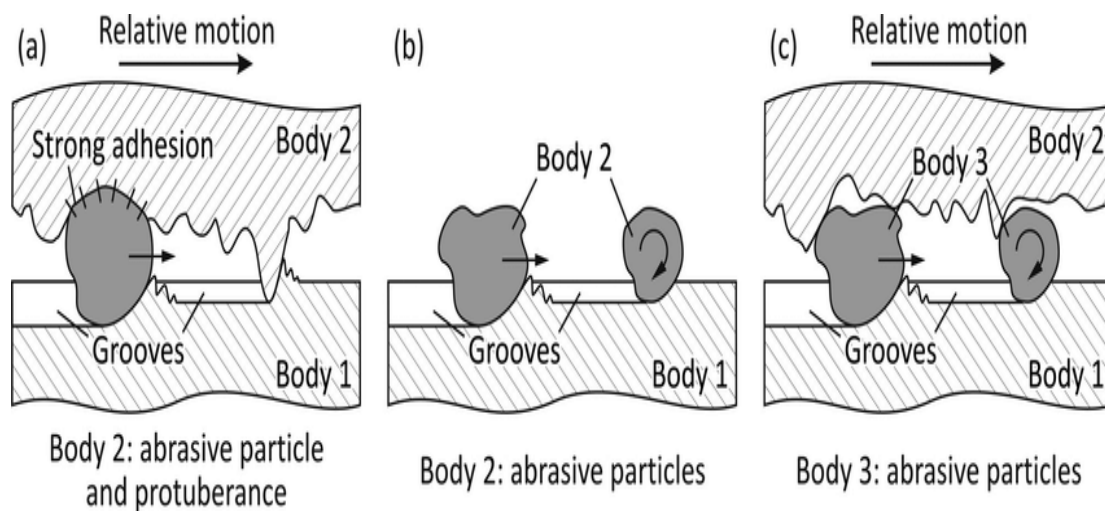
Figure 3 (a) Abrasive wear types, (b) two-body and (c) three-body abrasion [11]

Two-body abrasion occurs when hard particles remove surfaces from the opposite surfaces. This phenomenon is usually performed during the cutting operation in machining processes. Three-body wear usually occurs when the hard particles have no specific location and are free to move and roll over the other surface. There is another classification of wear that can be considered as open and closed [12]. Open wear occurs when the abrasive particles have no sufficient hindrance from the other surface, and then the material is removed in different ways. On the other hand, in closed wear, the abrasive particles are kept in contact. Finally, three commonly known behaviors have been proposed for abrasive wear, as follows:

i)   Plowing

ii)   Cutting

iii)   Fragmentation

Plowing occurs when materials are pushed to the side on the striking of abrasive particles. The subsequent pass of abrasive material removes the material moving in the grooves. The cutting step occurs when the material is removed in small particles without moving to the sides, as in the plowing mechanism. Finally, fragmentation is the localized fracture on the striking of the cutting part. These wear behaviors are illustrated in figure 4. The spalling phenomenon occurs when the adjacent material is removed along with the material directly in contact with the cutting part.
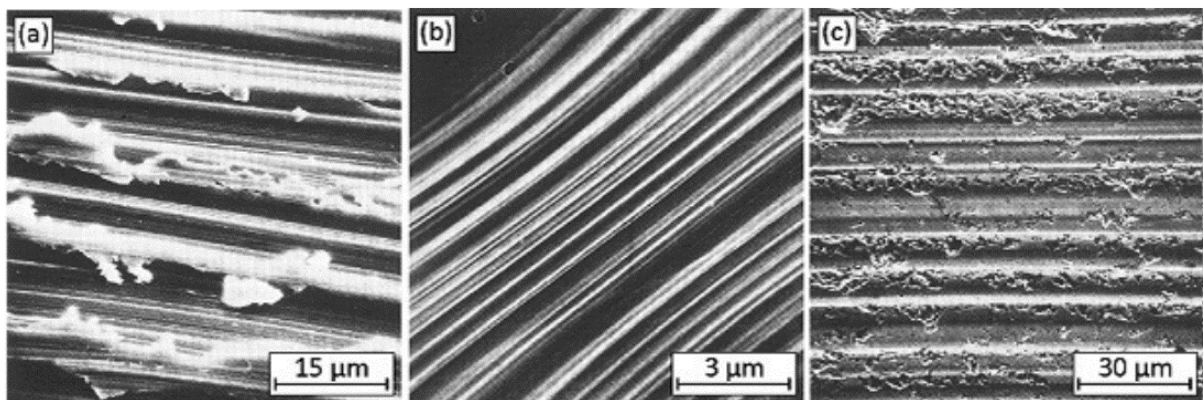
Figure 4 The appearance of surfaces worn caused by different abrasive mechanism types: (a) ploughing, (b) cutting, and (c) fragmentation [11]

The material removed during the abrasive wear can be calculated by the mass loss due to the Taber Abrasion Test using ASTM D 4060 or ISO 9352.

The overall volume of wear, V, can be calculated by the following formula,

$$V = \alpha\beta \frac{WL}{H_v} = K\frac{WL}{H_v}$$

W is load, α is the shape factor (value $\approx$ 0.1), β is a degree of wear (typically 0.1 - 1.0), L is the sliding distance, K is a wear coefficient, and H_v is the hardness level.

3.2.2 Adhesive wear

The term adhesive is related to the ability of a surface to hold itself together and form a surface bond with the other surface with which it is in contact. In general words, adhesive wear occurs when the material is pressed against the other during the sliding phenomenon, and the surfaces adhere to each other. Different materials have different surface attraction levels, which can be amplified by enhancing the magnitude of the surface energy. Each solid has some magnitude of attraction with the other solid. However, this attraction phenomenon is varied by oxide films, contamination, and lubrication, which naturally interfere with surface attraction. If absorbed species occur, a spontaneous exothermic reaction produces a film with a low surface energy level [13]. When adhesive wear occurs, the surface roughness increases and lumps are created, influencing the final wear behavior (see figure 5).
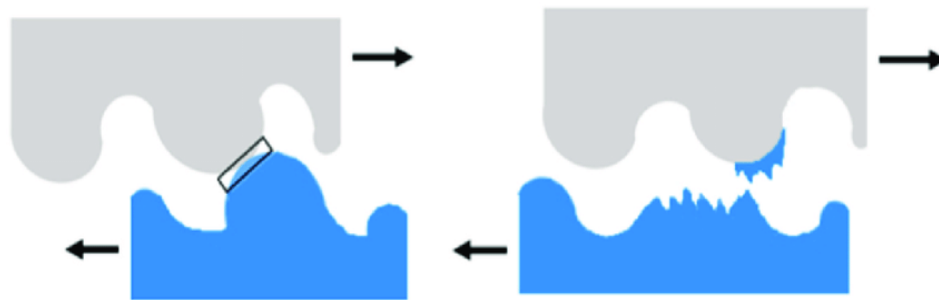
Figure 5 Example of adhesive wear [14]

The weld junction created in adhesive wear is due to electrostatic forces, particularly Van der Waals forces. If the created junction becomes stronger than the bulk properties of any of the materials in contact, the shear stresses can cause the material transfer. This phenomenon can be temporarily in the form of a disturbance of the surface integrity of the material or a full transfer of the film from the surface. The phenomenon of adhesive wear is usually observed in high molecular weight substances like polymers [15]. Under steady-state, the polymer flow originates adhesive wear similarly to metals where the material removal is proportional to the load [16].

3.2.3 Fatigue Wear

Fatigue wear is a type of wear where several cycles are needed to generate debris. The fatigue process in metals may prompt the generation of surface and subsurface cracks, which results in severe damage after a critical number of cycles, such as large fragments leaving the surface [17], [18]. Two mechanisms can distinguish fatigue wear as illustrated in figure 6 [19]:

a) High-cycle fatigue

b) Low-cycle fatigue
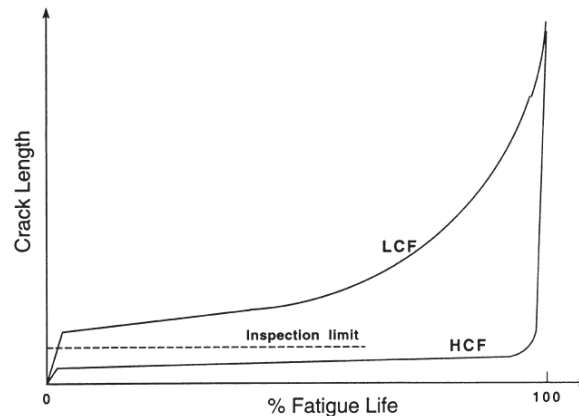
Figure 6 Schematic indicating the conceptual differences between HCF and LCF [20]

The component life is relatively long in high-cycle fatigue, as the number of cycles before failure is high. In this mode, the cracks are initiated because of preexisting micro defects in the material, near which the local stress may surpass the yield value. However, the macroscopic contact is in the elastic regime. The initiation of a crack is due to the accumulation of plastic strain around inhomogeneities [21].

The component fails faster in the low-cycle fatigue, as the number of cycles before failure is low. In this case, the wear particle is generated over the course of accumulated cycles [22]. During the first cycle, the wear debris is not generated; rather, only the shallow grooves due to plastic deformation are formed, as discussed in [23]. The plastic strain exceeds a critical value, and the fracture occurs only after a critical number of cycles. Crack propagation has three stages: crack initiation, growth, and post-critical stage when the catastrophic failure occurs [24]. Most of the component's lifetime is occupied by the first stage, with initial cracks around 2-3 μm and lower [25].

3.3 Wear characterization techniques

Surface engineering and coatings for the surface modification of various mechanical components and tools have been proved to be a successful way of improving their performance [26], [27] for several decades. However, the quality of such modified elements remains a subject of complex triboanalysis, using sophisticated tribotesting methods. Absolute testing of machines and equipment is usually a multilevel and multiscale task [28]–[30]; therefore, the

tests are mostly simplified to model a real tribology contact. Some of the standard wear testing methods and geometries used to analyze non-lubricated sliding tests are pin-on-disc, block-on-ring, and crossed cylinder. The pin-on-disc is the most frequently used test system in non-lubricated non-abrasive wear research as this test is simple and only a few parameters such as load, sliding speed, and distance need to be controlled to obtain the desired result. However, the results might be different in actual industrial applications. Therefore, other tribological tests should be encouraged to mimic the real contact condition, such as block-on-ring and crossed cylinder. The sliding wear behaviors of materials in different simulated conditions are evaluated by the Block-on-Ring (ASTM G77) technique, allowing reliable ranking of material couples for specific tribological applications [31]. In contrast, the crossed cylinder wear test evaluates thin coatings of metal forming and cutting tools [3]. Podgornik et al. [32] compared different test methods for evaluation galling properties of surface engineered tool surfaces. Their investigation revealed that the load-scanner is a useful tool for evaluating engineered surfaces meant for cold forming operation. In contrast, the cylinder-on-cylinder test was limited to a single wear track. However, the pin-on-disc was one of the simplest configurations but was restricted due to fixed load and a single wear track. Among various wear characterization techniques discussed above, pin-on-disc and crossed cylinder wear tests are described in detail.

3.3.1 Pin on Disc

The use of pin-on-disc configuration is essential to investigate the wear phenomenon in solid material. The calibration is crucial in this scenario as the results of this configuration have been observed to differ from the theoretical data. Different results are obtained in the arrangement of rotating pins and stationary pins under the same load, but the speed being different. The rubbing medium's temperature increases with time, which eventually reaches a specific value on establishing steady-state conditions; the values continuously vary. The contradictions can be explained by accurately calculating the bulk and flash temperature at the contact area [33]. The pin-on-disc wear tests are widely used at laboratories due to their simple arrangement. Some phenomena, however, which affect the test findings are still markedly ignored. If the test is not restricted to a single rubbing pass, the pin and the disc aggregate the rubbing heat. Its bulk temperature increases accordingly until they stabilize to a specific thermal temperature.

Experimental Setup

A schematic diagram of pin-on-disc has been shown in Fig 7a and the position of the electrostatic sensor in fig 7b.
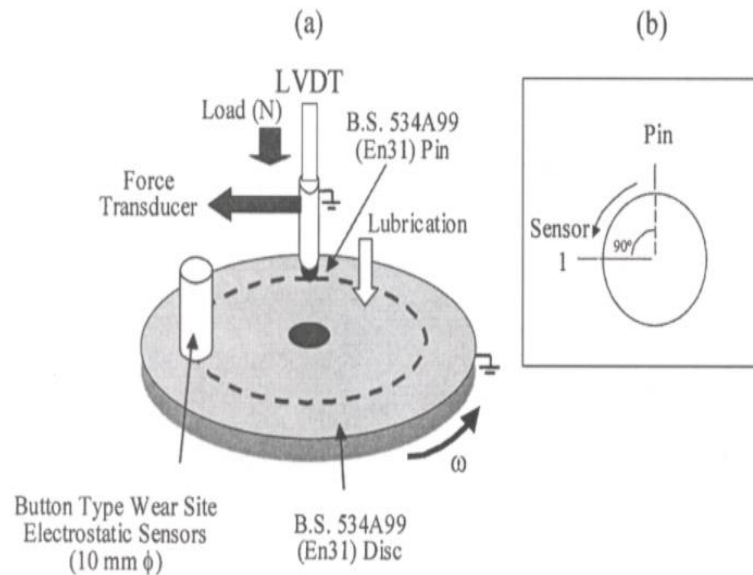
Figure 7 (a) Schematic diagram of pin-on-disc tribometer test up (b) position of the electrostatic sensor [33]

The load is applied by air cylinders or dead weight through the stationary rod to the rotating specimen. The frictional factor is measured by a load cell mounted on the stationary rod. The shaft rotational speed is controlled by a dc servo motor with a controlled RPM system. The temperature of the pin can be calculated by the thermocouple welded on the pin. The amount of wear is measured with a differential transformer and a data acquisition system. Infrared microscopy is a suitable technique to measure infrared temperature.

3.3.2 Crossed cylinder techniques

ASTM G 83-86 is a standard test used for the wear tests with a crossed-cylinder apparatus. This test covers ranking metallic couples as resistance to slide wear using the crossed cylinder apparatus. In this test, wear occur at the contact between a rotating cylinder and a stationary cylinder, which have their long axes oriented to each other [34]. For the same material, the wear rate is the volumetric loss in cubic millimeters of stationary and rotating cylinders. For the different materials, the wear test reported the total volumetric loss in a cubic millimeter for the rotating and stationary test cylinders as well as the volume loss of each cylinder separately. The type of test procedure specifies the manner of results recording. The amount of wear in

any material generally depends on various factors such as sliding speed, applied load, sliding distance, materials, and environment. This test provides standardized conditions to determine the relative wear rates of different metallic couples. However, it is limited as it cannot simulate the wear behavior of coated cutting and forming tools, which is close to industrial operations. However, the modified crossed cylinders test where one of the cylinders moves about the other cylinder's length solves those issues. It has all the qualities mentioned below and used by Sato et al. [3], Zhu et al. [4], Gerth et al. [5], Aiso et al. [35], Heinrichs et al.[6], Olander et al. [36] throughout the different timelines.

The wear test for structured tools should maintain the following features [3]:

- Should be able to assess the relation between sliding distance and wear depth (or wear volume) within a thin coated layer thickness of several microns.
- To cope with the alteration of testing conditions such as load, sliding velocity, lubrication, and mating materials.
- The structured tool should always slide over the new surface of the mating material, as seen in the cutting or forming application (see figure below).
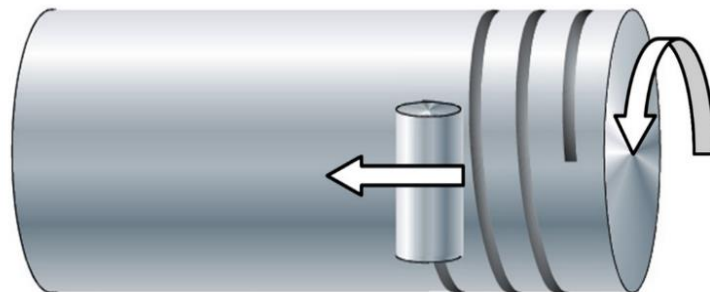
Figure 8 Schematic view of the contact situation in the sliding contact of crossed cylinder setup [36]

Sato et al. [3] used seven coatings on HSS against the carbon steel and commercially pure copper, used as the counter material. They tested the suitability of using a crossed cylinder wear test to evaluate the wear behavior and the tribological properties of coated forming tools examined under conditions close to industrial operations, which was impossible using a scratch test. They introduced a parameter, λ_m, which is the effective mean wear rate to express the coating's anti-wear performance. The relation between the effective mean wear rate and the sliding speed was different for each coating [3]. Moreover, the result showed that the technique could screen the improper coating tool as flanking or partial flanking occurs at the early stage of the test.

Later, Zhu et al. [4] used the same wear test technique to investigate the tribological properties of CN and TiCN coatings. CN and TiCN coated cylinders (representing the tool) of Ø 12 mm were fixed at the end of a loading apparatus. Then, they were forced against another cylindrical sample made of an AISI 1019 steel rod of Ø11.5 mm and 100 mm in length (representing the work material), rotated on a program-controlled lathe. The test was carried out in dry lubricated conditions at room temperature of about 25°C. A 35.3-88.2 N load range was maintained, while the sliding speed of 0.23 and 0.37 m/s between the contact surfaces was selected [4].

The friction coefficient was found to be constant when the load was raised. However, the depth of wear scar was increased with the load. There was a sudden increase in wear scar depth under dry conditions when the load was raised to 70.6 N, which was likely caused by the coating being worn through. The generation of wear debris was observed, which indicated the material transfer between the counter surfaces [37], resulting in a higher coefficient of friction and wear depth [4].

They concluded that the greater wear scar depths were the result of higher loads. The performance of coatings during the sliding wear test strongly depends on the type, thickness, and hardness of the coating. As described previously, crossed cylinder technique is reliable and could be used as an inexpensive laboratory technique [4].

Moreover, Gerth et al. [5] and Aiso et al. [35] used the crossed cylinder wear test to simulate the material transfer in the milling operation. The same experimental setup was used as explained earlier; the only difference for this test was the intermittent sliding. The detailed parameters of the test are shown in table 1. A quite steady coefficient of friction was observed as the load and the friction force followed each other closely during each contact [5].

Table 1 Intermittent sliding test conditions [5]

Test Parameter	
Sliding speed	125 m/min
Mean normal pressure	50 N
Duration of each contact	35 ms
Number of contacts	50
Sliding distance per contacts	0.07 m
Total sliding distance	3.5 m
Total test duration	26.8 s
Lubrication	None (dry)
Atmosphere	In air
Temperature	20°C

All coating contact tracks showed a similar appearance when the surface analysis was done using SEM. Each track consisted of two areas with differences in contrast—a darker spot in the middle and a brighter, more diffuse area surrounding it. The brighter area was always larger than the darker area when SEM compositional mode was used (see figure 9). Cross-sectional SEM studies of the tracks verified that all coatings were intact and virtually unworn as the HSS substrate material was not exposed in SEM [5].
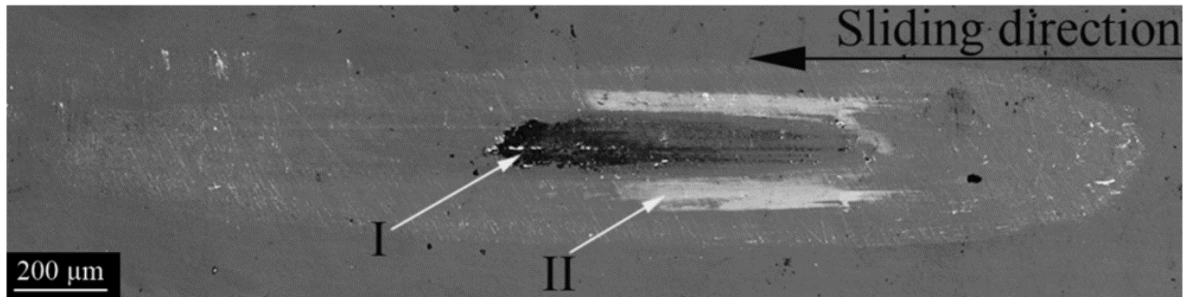
Figure 9 Contact track showing two different areas, dark (I) and bright (II), of adhered material imaged using the SEM compositional mode [5]

Since the amount of adhered material on the cylinders was believed to have a strong influence on the contact conditions, the size of the covered area was quantified. The area measurements were plotted against the mean friction value for individual contact tracks and coatings. The friction coefficients were in the interval from 0.8 to 1.1 for all coatings tested during the intermittent sliding test. It was constant or slowly increasing during a single test consisting of 50 engagements. Measurements in the intermittent sliding test showed an increase in friction coefficient with an increase in contact area covered with the layer of oxidized steel constituents [5].

Aiso et al. [35] concluded in their experiment that the mode of material transfer was strongly dependent on normal load and sliding speed. The high load was proved to be the most important factor to accurately simulate the mode and area of material transfer occurring in milling. The diameter of the work material cylinder influences the shape of the contact mark. However, it does not influence the mode of transfer. Thus, smaller diameter work material can reduce cost and ease handling both tests and analysis.

Recently, crossed cylinder wear test was used by Olander et al. [36] to investigate the initiation and propagation of tool wear in the turning of titanium alloys. A cylinder of ø 5 mm, L 30 mm of cemented carbide grade H13A was used as tool material, while a cylinder of ø 57 mm, L 160 mm of titanium alloy Ti6Al4V was used as work material. The tests were performed at

interrupted and continuous modes. A feed of 0.84 mm/rev was implanted so that the tool cylinder can meet fresh titanium in each revolution. A high load of 700N was applied to cause significant plastic deformation of the work material [36].

A plastically deformed track was seen in the titanium, with typical ridges alongside it. The deformed contact track is about 300 µm wide and more than 2 µm deep, clearly distinguishable from the surface roughness resulting from turning the cylinder. A rapid friction coefficient increase occurred immediately after start-up, and a peak was recorded at the end for each test, as seen in figure 10. A stable friction coefficient of 0.25 was observed, as both load and friction force were very stable, resulting irrespective of test mode and accumulated sliding length [36].
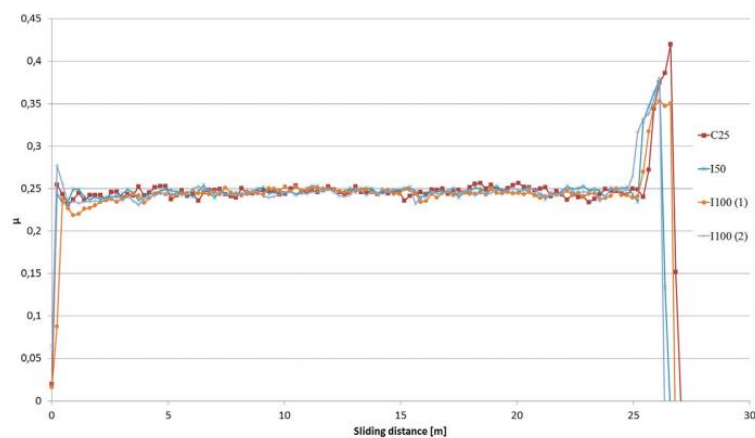
Figure 10 Coefficient of friction calculated from load and friction force measured during C25 and all subtest with a 25 m sliding distance

3.4 Self-lubricating coatings

The use of coatings is constantly increasing to improve the tribological properties of components such as metal cutting and forming tools. The bulk material of a machine element or component is selected to meet the requirement for stiffness, strength, formability, cost, whereas coating carries all the other functional properties [38]. Therefore, the coating is one of the effective ways of improving the friction and wear resistance properties. However, the main aim of applying the tribological coating is to obtain an expanded lifetime. There are, yet, several other positive impacts.

- The improved wear resistance is utilized to increase the cutting speed and productivity rather than prolonging tool life.

- Friction reduction often results in reduced energy consumption. Moreover, in some cases, a lowered friction might help to exclude lubrication or cooling stages.

- Anti-sticking agents may be omitted in forming tools and many sliding applications.

Friction causes tool passivation, degradation of workpiece surface quality, and energy loss during a cutting operation. Manufacturing alone takes up about 31% of total energy consumption in developed countries like Europe and America [39]. In manufacturing, to reduce friction and wear, cutting fluid is applied. However, the production, application, and disposal of cutting fluid will cause serious pollution, seriously damaging the ecological environment and endangering human health. Cutting tools are deposited with self-lubricating coatings to solve the problem.

Self-lubricating tools are prepared by fabricating a lubricating coating on a traditional tool surface. The turning tool was coated with MoSx-based self-lubricating coatings by using magnetron sputtering technology [40]. COF and cutting force of self-lubricated tools were way lesser than uncoated tools, and wear resistance of tool was increased. The drill bit coated with MoS2/Ti (self-lubricating coating) had a service life that was 2.1 times longer than that of the drill bit coated with TiN and was 2.8 times longer than that of the drill bit coated with TiAlN [41].

WS2 solid lubricant film, when deposited onto the micro-textured TiAlN coated surfaces, showed that the lubrication between the tool and chip is improved due to the lower shear strength of WS2 self-lubricating coating [42].

Self-lubricating coatings such as W-S-C, DLC with W, and DLC with SiO will be investigated using crossed cylinders test in this study.

3.4.1 W-S-C Coating

Common drawbacks of pure TMD are low load-bearing capacity and low adhesion to the substrate. There are many different possibilities to improve the tribological behavior of these coatings. Doping the TMD film with C is one of the most successful ways to overcome the above-discussed problem. Alloying of a WS2 with non-metals like carbon could improve mechanical properties and adhesion of the films on steel substrates; moreover, it is possible to tune the coating microstructure by metal content.

Todor et al. deposited W-S-C coating on a steel substrate by R.F. magnetron sputtering using Edwards E306A equipment [43]. The average COF generally decreased with the increase of the load, reaching values as low as 0.05.

One of the major challenges in the deposition of these coating is a compositional variation mainly related to variation in S/W ratio, which can strongly affect the coating's tribological performance. Surface location is essential during the deposition of W-S-C coating in the chamber. This coating has been placed on different surfaces ranging from large and smooth surfaces to more complex surfaces as in mold and dies.

Todor et al. utilized another methodology to deposit coatings by unbalanced magnetron sputtering in a semi-industrial unit in a closed field using a volume of 275dm3 [44]. The following conclusions were observed [44]:

- Target to substrate distance has a significant effect on the composition of the coatings, with the longer distances resulting in a higher S/W ratio and a higher overall amount of sulfur. In contrast, lower S/W ratios and higher C contents resulted in denser microstructures and increased hardness.

- With increasing the loads and/or the testing temperature, the formation of WS_2 rich tribofilms accelerated with a subsequent reduction in friction.

- High friction was observed when testing was carried out in a vacuum with steel counter bodies due to severe adhesion that led to preferential wear.

Generally, C-doped TMD based nanocomposite thin films have shown promising results with good tribological behavior in diverse environments. Moreover, there is a lack of information

regarding the deposition of C-alloyed transition metal dichalcogenide coatings deposited in larger (semi-) industrial deposition units.

To upscale the deposition process of W–S–C thin films with the self-adaptive tribological response, deposition of W–S–C coatings was performed in a closed field unbalanced magnetron sputtering using DC supply.

3.4.2 DLC coating with W

Carbon-based coatings are well established in tribo contacts such as biomedical devices where low wear ($<10^{-16}$ m^3/Nm) and friction (COF<0.2) are sought out, particularly diamond-like carbon coatings (DLCs). Since in-service conditions provide hindrances in exhibiting the required tribological properties for pure DLCs, their service temperature is limited to 200°C owing to their fast oxidation. As a remedy to this, several kinds of research have been carried out on novel deposition techniques along with gradient interlayers to enhance adhesion and alloying of DLCs with metals such as carbide formers (Ti, Cr, F, W) and non-carbide formers (Ag and Cu). Out of these elements, W is the most studied to offer an increased lifespan with improved tribological properties at higher temperatures [45], [46].

Evaristo et al. [45] studied the effect of tungsten doping on four different DLCs deposited by direct current magnetron sputtering in reactive and non-reactive atmospheres with Ti interlayer under similar conditions with two variations: the power to tungsten pellets and CH4 introduction in the chamber. Two hydrogenated coatings with 7 and 23 at.% of tungsten alloying were deposited (a-C:W-7(:H) and a-C:W-23(:H)), whereas, for non-hydrogenated 10 and 28 at.% of W was incorporated in the coatings (a-C:W-10 and a-C:W-28). For tribo-testing, the SRV test was carried out with a stoke of 1mm, 40 Hz frequency, and 50 N load for 42 minutes for 200,000 passages in wear scar center. Whereas pin on disk test was performed for 5000 laps with 0.2 ms-1 sliding conditions under 5 N load with a wear track of 7 -15 mm. Deposited coatings were reported to have free tungsten in the morphology with nano-crystallites of WC embedded in the carbon-rich matrix. The hardness of the coating exhibited as the tungsten increases improvement from 10 to 15 GPa. Figure 11 shows that friction coefficient and wear rate increased linearly when temperature increased from room temperature to 300 °C. For alloyed coatings in the dry test case, COF rose from 0.4 to 1.1 and wear rate from 1 to 6.5 x 10^{-6} mm^3/Nm [45].
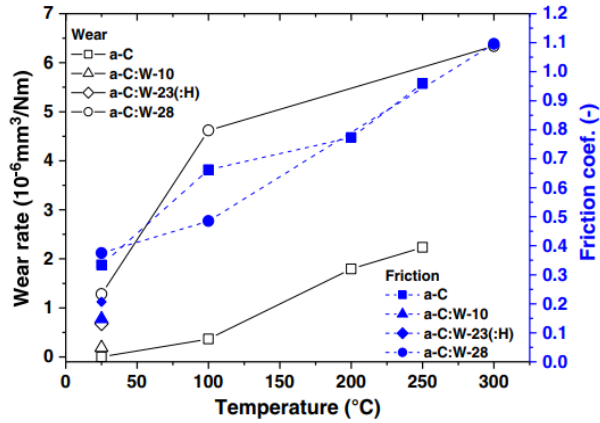
Figure 11 Wear rate and frictional confidence as a function of temperature [45]

In another study performed by Evaristo et al. [46], the tribological properties of W doped DLCs deposited by a hybrid configuration of direct current magnetron sputtering with high power impulse magnetron sputtering (HiPIMS) were compared. This hybrid configuration deposition leads to dense morphology where the shadowing effect was hindered. Coatings that demonstrated lower wear rates at room temperature and 150 °C were HiPIMS depositions. It can be observed from figure 12 that coatings deposited with HiPIMS have very low COF of ~ 0.3 at RT and ~ 0.1 at high temperature, with wear rates less than 2.0 x 10^{-7} mm^3/Nm in both cases.
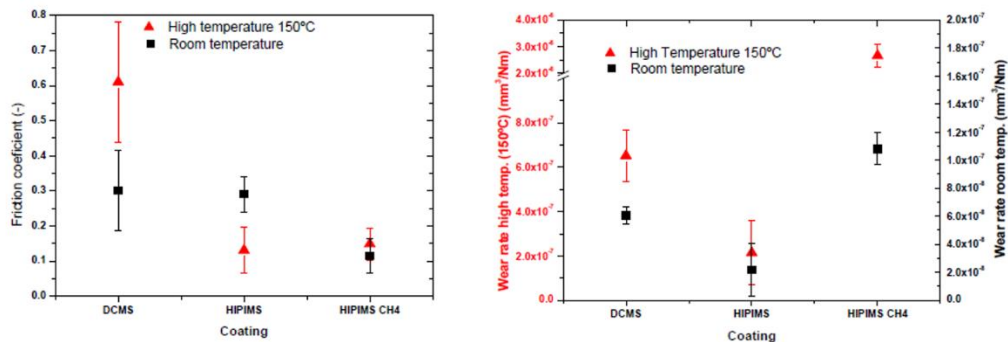
Figure 12 a) Average friction coefficient at high (150 °C) and room temperature (b) Specific wear rate for both temperatures [46]

3.4.3 DLC coating with Si-O

Silicon is an important element incorporated into DLC to overcome the starting drawbacks, including intrinsic compression stress, mechanical resistance, and good adhesion. When both oxygen and silicon incorporate into DLC, a substantial structural modification has been observed. Some authors claim hydrogen can stabilize the carbon network while the silicon

network can be stabilized by oxygen. Silicon oxide containing DLC presents interesting tribological, mechanical, and optical properties with high thermal stability and fracture toughness [47]–[49]. The high silicon content up to 29% and annealed at 500 degrees Celsius in air exhibit high friction due to cracks on the surface by Choi et al. [50]. Venkatraman et al. [51] studied film wear rate from the low to absolutely high 10^{-6} mm^3/Nm when it is annealed from 400 °C to 500 °C.

Evaristo et al. [52] studied the effect of modifying silicon and oxygen content on a-C:Si:O coating with magnetron sputtering in a reactive atmosphere with Ar and O$_2$. Silicon content was increased to a maximum of 24 at. % at maximum power applied to silicon target; oxygen was increased to a maximum of 27 at. % by adjusting oxygen flow in the system. Increasing Si content showed two distinct trends in the hardness a-C:Si:O coatings as can be seen in figure 13, hardness decreased for Si content lower than 10 at. %, then it started increasing. Increasing O content caused a reduction in hardness and young modulus values [52].
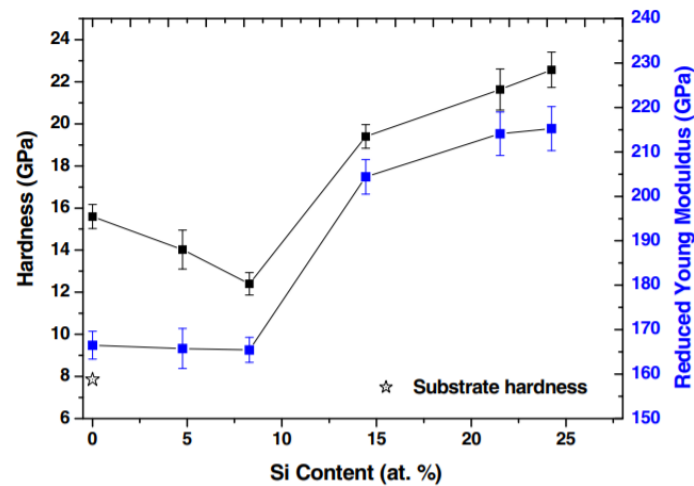
Figure 13 effect of silicon content on hardness and reduced Young Modulus in a-C:Si coating system [52]

Evaristo et al. [52] fixed Si/C ratio to approximately 18%, while studying friction behavior with increasing O content. Table 2 shows the chemical composition obtained by electron dispersive spectroscopy (EDS) of the coatings used. Figure 14 shows the effect of increasing O content on average COF; favorable results while performing the tests using pin-on-disk were attained with COF values of 0.09 to 0.03 for the lowest and highest O content, respectively [52].

Table 2 Chemical composition obtained by EDS of the coatings deposited with increasing O content [52]

Power on Si target (W)	O₂ flow (sccm)	C (at. %)	Si (at. %)	O (at. %)	Ar (at. %	Si/C (%)	O/Si	Thickness (μm)
365	4.1	75.7	13.8	7.6	3.0	18	0.6	1.0
377	6.9	71.8	12.8	12.4	2.9	18	1.0	1.0
380	9.6	67.4	12.0	18.1	2.2	18	1.5	1.2
395	12.4	68	10.6	19.0	2.4	16	1.8	1.2
420	16.5	60.7	11.2	27.1	1.0	18	204	1.2
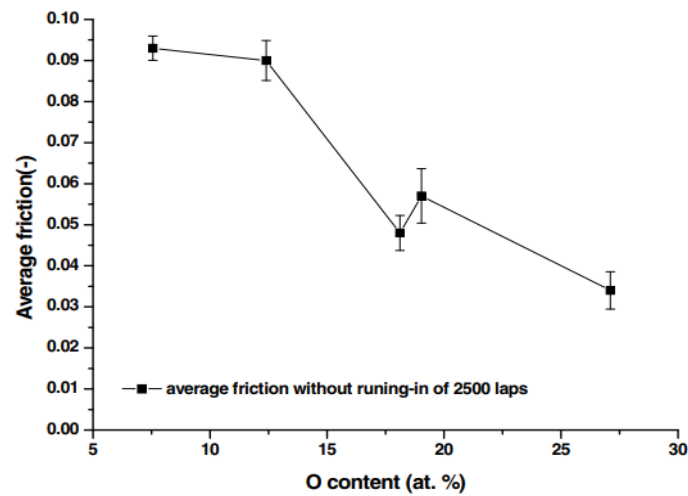
Figure 14 Steady-state COF with increasing O content, using pin-on-disk experiment [52]

Evaristo et al. [52] showed a COF reduction from 0.17 for an unalloyed coating to 0.03 for a-C:Si:O system with the highest O percentage. XPS results suggest that oxygen has preferential bonds with Si, forming Si-O-C mixed bonds in an amorphous carbon matrix [52].

4. Research gaps

During various machining operations, material transfer between work material and tool occurs, especially in dry contact. In metal forming operations, it may lead to galling [32]. In contrast, in the metal cutting operation, the adhesion at the tool-chip interface strongly impacts the energy spend [53], thus reducing tool life. Furthermore, small alterations in the work material's chemical composition can occur due to the work and tool material's mutual adhesion properties. So, the study about the combination of successful tools and work material is of great interest. During the tool-chip contact, high thermal and mechanical loads and high deformation

and sliding velocities are involved in the real cutting process [54]. Therefore, the more these parameters are involved, the better is the result.

Furthermore, Hedenqvist et al. [55] conclude that the continuous introduction of a new counter material surface is essential than an unoxidized state to obtain relevant contact conditions. Several studies have been done until now to replicate the contact conditions between the tool and workpiece. However, all those research have been limited to the hard-coated tools, though the advantages of the self-lubricating coated tools for cutting and forming operation are numerous. This study will use the knowledge of the sliding test on crossed cylinders for the self-lubricated coatings replicating the real contact condition to fill all these research gaps. Moreover, the relation between the friction coefficient and the microstructural changes occurred during the test, which later can be used to modify and improve the coatings.

5. Objectives

The main aim of this master thesis project is to evaluate the relationship between the friction coefficient and the microstructural changes which result from the application of a constant force in the sliding contact during crossed cylinder testing in dry contact. Three different coated samples will be used for this study, in all cases coatings developed for low friction applications. The following steps will be taken to achieve our objective:

1. Fundamental characterization of the self-lubricating coatings
2. Preparation and optimization of the testing rig (cylinders, dynamometer, turning machine, calibrations)
3. Performing friction tests using crossed cylinder geometry
4. Characterization of the coated sample after tribological testing (microstructure, mechanical properties, sliding mechanisms)
5. Analysis of the results and conclusion.

6. Methodology

The project consists of four tasks. Task 1 is dedicated to the coating of the samples, where different self-lubricating coatings are deposited on the substrate, whereas, in Task 2, calibration of the equipment for the modified crossed cylinder test was carried out. The tribological testing of the coatings was done as task 3; Task 4 corresponds to the characterization of the coatings and tested samples.

6.1 Coatings

Different coatings were deposited on metal cylinders in the IPN facility. Cathodic sputtering in a Teer Coatings Ltd. UDP 650 was used, utilizing four targets (see figure 15) with the dimensions of 380x175x10 mm. Before deposition, the targets and substrates underwent an ionic cleanup for 20 minutes .
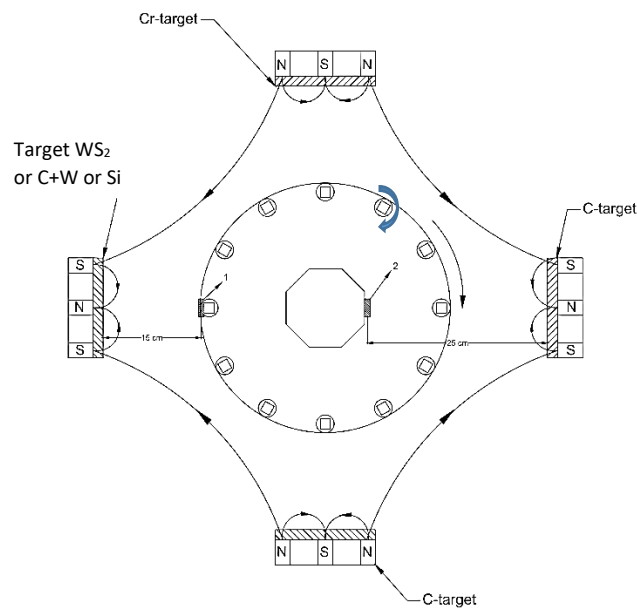

Figure 15 Schematics of deposition process [56]

For W-S-C deposition, four targets: two carbon - C, one tungsten disulfide – WS_2, and one chromium - Cr (metallic interlayer) were utilized. The targets were connected to DC power sources, and the working pressure was maintained ~0.6 Pa. It was possible to achieve several chemical compositions using this configuration.

DLC-W was deposited utilizing four targets: two carbon - C, one C with 14 tungsten pellets - (C+W), and one chromium - Cr (metallic interlayer). The tungsten pellets were set within the favored erosion zone of the target. For the deposition, the power within the C targets was kept consistent and to get the content in $\pm$ 10% at. W in the coatings, the power on the C+W target was regulated as performed in previous research (literature review).

Four targets: two carbon - C, one silicon - Si, and one chromium - Cr (metallic interlayer), were used to deposit DLC-Si(O). The power on the target of Si was adjusted as performed in previous research (literature review). The power in the two graphite targets was maintained identical to the remaining depositions. The power applied to the target of Si controlled the Si content, simultaneously with the addition of O_2 to the discharge atmosphere. The O_2 content was adjusted by controlling the partial pressure of the air gases and O_2 inside the chamber.

In addition to the coatings mentioned above, DLC was also coated in the substrate so that additional tests could be carried out, which could help better understand the coatings in the new tribological testing system. Steel cylinders (Ø 20 x 50 mm) were utilized as substrates for the tribological test, so it is essential to put the substrate carrier to pivot around its axis (Figures 15 and 16). Silicon wafers and steel discs were also coated for morphological, chemical, and mechanical examination of the coating, as appeared in figure 16.
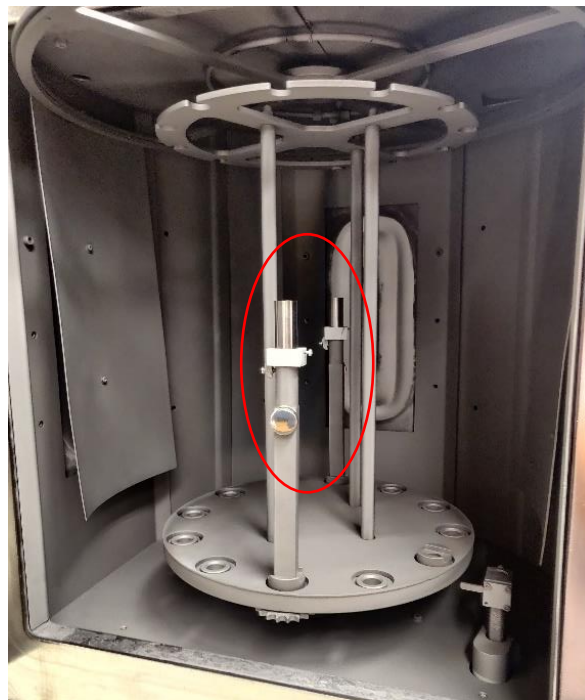
Figure 16 Placement of cylindrical sample for deposition with a special holder

6.2 Calibration of the equipment

The equipment was calibrated before the actual test. Standard weights (3, 5, 10, and 15 kg) were used to check the force in all axes read by the 3-component piezoelectric force dynamometer, as seen in figure 17a. The distance between the contact point and vertical (front) face of the dynamometer was also varied (20mm, 35mm, and 50mm) to check the accuracy in the readings as the standard distance for the device is 35mm (figure 17b). In addition to that, the calibration was carried out by inverting the dynamometer. The actual test will be used in inverted format to align the test cylinder with the center of the counter cylinder, as seen in figure 18. Moreover, for all the tests, the accuracy of the result was in the range of ±5%.
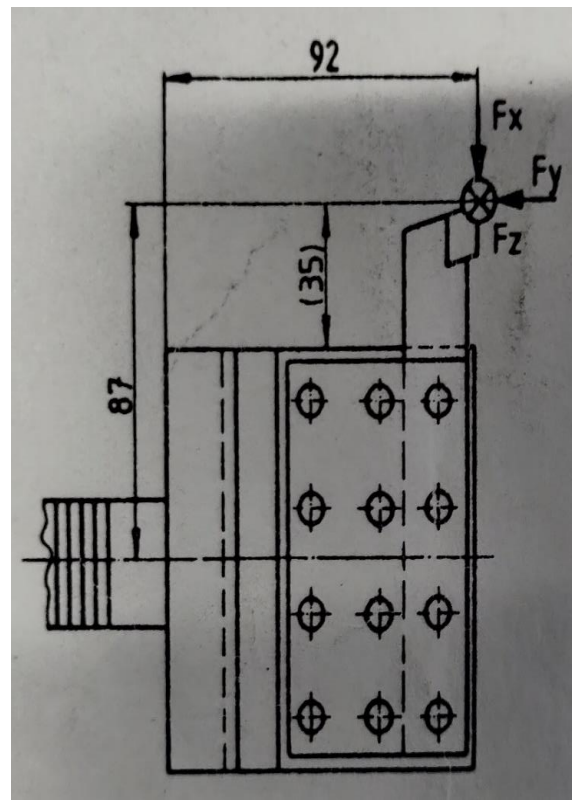
(a)   (b)

Figure 17 (a) Calibration with standard loads, (b) Specification of dynamometer

6.3 Crossed cylinder test

A modified crossed cylinder test was used for the project, where the small cylinder was spring-loaded against the larger rotating cylinder at right angles to the latter in the sliding test (see Fig. 18). After the initial load was applied by the spring, a compressed air system applied the final

workload (F_x). The tests were carried out with loads of 30N, 70N, 90N, and 100N. The contact pressure was varied to see a significant difference in the coated cylinder mechanical response and the counter-body assembly, that is, in the deformation of the counter-body. However, to avoid plastic deformation at the contact of both cylinders, the maximum contact pressure between surfaces was limited to 1 GPa.

Figure 18 Experimental Setup: Mechanical lathe (1), Dynamometer (2), Coated cylinder (3), Counter cylinder (4), and transparent panel to block the air (5)

This experiment was carried out at IPN facilities. A triaxial dynamometer was installed in a mechanical lathe machine, and a sample carrier was used to apply the normal force to the coated cylinder (Figure 18 (3)). A variable preload (range 20 N to 40 N) was applied to the cylinders using the mechanical lathe and the final value of the F_x, adjusted using the compressed air. Tool steel cylinders (Ø 20 x 50 mm) were coated with WSC, DLC-W, and DLC-Si (O) coatings. A stainless-steel bar (Ø 50 x 500 mm) was used as a counter-body for the crossed cylinder tests. All sliding tests were carried out without applying any lubricant (dry condition) in room conditions (temperature and humidity). A conventional lathe was used where a sliding speed corresponding to the pin-disc test speed (0.1 m/s) was used in all tests, with a feed rate of 0.79 mm/rev. For most of the tests, the sliding distance was 5000 mm but to see the behavior of friction coefficient; later, the sliding distance was increased to 10000 mm and 15000 mm. The 3-component piezoelectric force dynamometer (Type 9257A, KISTLER, Switzerland) was used to measure the normal and frictional forces.

6.4 Characterization technique

Nanoindentation tests (NanoTest, Micro materials, Wrexham, UK) were performed using a Berkovich diamond pyramid indenter to measure the hardness of the coated samples. A map was made using 7x7 indentation with a 5 microns distance between them. Two sets of different loads of 5mN and 10mN were used to measure the hardness where the indentation was within 10-15% of the coatings' thickness.

The chemical composition and thickness of the coatings and counter cylinder were analyzed using scanning electron microscopy (SEM) with a dispersive energy detector (EDS). The detailed characterization of the tested samples was performed using an intelligent cylindrical sample holder design as shown in figure 19, which made it possible to mount the coated cylinder directly in the scanning electron microscope (FESEM Zeiss Merlin, Oberkochen, Germany), to analyze the wear surface made on the test. Oxford X-Max 20 Silicon Drift Detector with a detector size of 20 mm2 was used for energy dispersive spectroscopy (EDS) analysis. For the chemical composition, the magnification of 10000x and the voltage of 10KV was used, whereas for the measurement of the thickness of the coatings, the magnification of 25000x and the voltage of 2KV was utilized.

The micro-Raman analysis was conducted in the backscattering configuration on a Horiba HR800 instrument using a 600 lines mm−1 grating and the 532 nm laser line from a HeCd laser (Kimmon IK Series, Japan). Moreover, a magnification of 50x was used.

Figure 19 Cylindrical sample holder used for analysis in SEM

Steps to be followed to use modified crossed cylinder test setup

A. Adjustment in the lathe

1. Fix the counter cylinder to the fixed head plate and use the tailstock to reduce the vibration of the cylinder.

2. Check the parallelism of the counter cylinder as shown in figure 20a.

3. Polish the counter cylinder to a surface roughness of $R_a < 0.25$ μm and check the roughness using roughness tester (Mahr Perthometer was used in this project) as illustrated in figure 20b.

4. Position levers to obtain the selected rotation value and feed rate (see figure 20c).

5. Position lever to select the carrier's movement direction and activate lever for automatic movement of the main carriage on it.

B. Using the dynamometer system

1. Fix the dynamometer to the tool holder of the main lathe carriage and check the inclination of the dynamometer in relation to the transversal carriage of the lathe, as shown in figure 20d.

2. Assemble the coated sample in dynamometer and bring it closer to the counter cylinder using the handle of the main carriage. Fix the ground cable to the charge amplifier.

3. Attach the cable to the load amplifier and signal amplifiers (see Figures 20e and 20f).

4. Attach the cable to the A-D converter and the signal amplifiers, then attach the USB cable to the A-D converter and the computer.

5. Check if the A-D converter unlocking pen drive is attached to it or not. After that, connect the signal amplifiers (see figure 21a).

6. Configure signal amplifiers: Transducer sensitivity (T), Scale (S), Filter (LP), Time constant (TC) as illustrated in figure 21b.

7. Connect the A-D converter and turn on the computer.

8. Launch the InstaCal and the DynoWare software and wait for the system to stabilize; time 30 minutes.

9. Select the edit acquisition option and enter the total value of the test time. Select the continuous cycle option, then select the location and the name of the file that will be generated.

10. Select the start acquisition option, fill out the technical details, and press OK.

11. Remove the information contained in the signal amplifier, then press the operate button on the signal amplifiers to start the data transmission. And start the dynamometer's cooling system.

C. Performing the friction test

1. Energize the lathe.

2. Start acquisition of force data in software and wait for 100 seconds.

3. Apply the value of the selected load against the counter cylinder by adjusting the spring system of the holder (20N, 30N, and 40N) and turning the micrometre collar of the cross slide. Record the numerical indication presented by the micrometre collar referring to the load previously applied, as shown in Figures 21c and 21d.

4. Adjust the air pressure needed to obtain the final workload (1bar = 10N), illustrated in figure 21e.

5. Wait for the load to stabilize (time: 100 seconds), move the dynamometer away from the counter cylinder, and reapply the force to confirm the readings.

6. Once the load to be applied is fixed, repeat steps B9, B10, B11, C2. Reposition the dynamometer according to the value previously registered on the micrometre collar and apply the air pressure.

7. Wait for the load to stabilize (time: 400 to 500 seconds).

8. Start the lathe main shaft rotation and the feed by operating the key switch on the main carriage, carry out the test according to the predetermined time.

9. Stop the rotation of the main shaft after the end of the friction test time. Wait for 100 seconds for the load to stabilize.

10. Stop the air pressure and move the dynamometer away from the counter cylinder.

11. Stop the acquisition on the software, press the operate button on the signal amplifier to stop transmitting the force data, and de-energize the lathe.

(a)

(b)

(c)

(d)
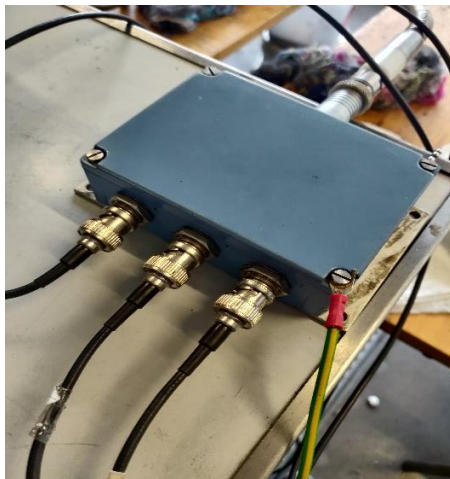
(e)

(f)

Figure 20 (a) Dial gauge for checking alignment, (b) Roughness tester for measuring roughness, (c) Levers of a conventional lathe, (d) Alignment checking of dynamometer, (e) Cables to load amplifiers and (f) Cables to signal amplifiers

(a)

(b)

(c)

(d)

(e)

Figure 21 (a) Configuration of A-D converter, (b) Configuration of signal amplifier, (c) Reading to adjust the load on spring system of the holder, (d) Micrometer collar reading for repeatability, and (e) Pressure gauge to adjust the final load

7. Results and discussion

This chapter is dedicated to the outcomes of the experimental methodology and their analysis. Similar to the previous chapter, this is divided into two parts: the tribological test and the other regarding the post characterization to support the result.

The chemical composition and thickness of the coatings and counter cylinder were analyzed using scanning electron microscopy (SEM) with dispersive energy detector (EDS) and presented in Tables 3 and 4. Nanoindentation tests (NanoTest, Micro materials, Wrexham, UK) were performed using a Berkovich tip to measure the hardness of the coated samples, and the results are presented in Table 4.

Table 3 Chemical composition of the counter cylinder

Fe (at. %)	Cr (at. %)	O (at. %)	Al (at. %)	Si (at. %)	Mo (at. %)
85.2	7.9	4.3	0.4	1.6	0.4

Table 4 Chemical composition, hardness, and thickness of different coatings

Coating	Chemical composition (at. %)					Hardness (GPa)	Thickness (μm)
	C	O	S	W	Si		
WSC	53.8	1.6	26.2	18.4	-	7.5	1.64
DLC	93.1	1.6	-	-	0.1	22	1.10
DLC-W	85.2	-	-	11.9	-	14	1.52
DLC-SiO	60.7	25.0	-	-	10.3	12	1.25

Three sets of tests were carried out for each load to check the test system's repeatability and obtain the average value of the coefficient of friction. As we can see from figure 22, the first set of test results for all the coatings is slightly different from the other two tests. This variation might have caused due to air leaking in the contact region from the holder attached to dynamometer, which was fixed in test two (T2) and test three (T3) by using a transparent panel to block the leaked air, see figure 18 (5). Therefore, the final COF for all tests was calculated using the result obtained in tests: T2 and T3.
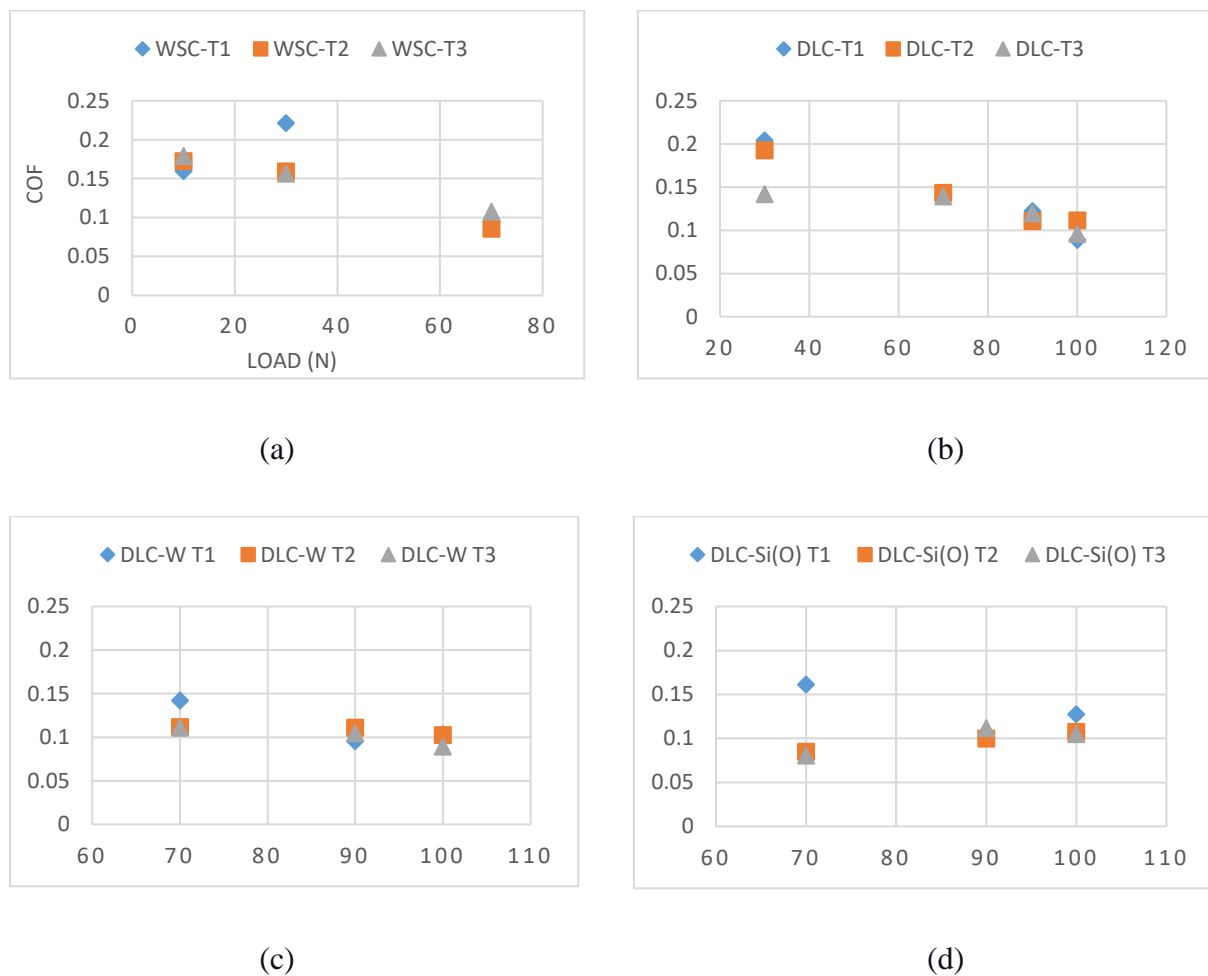

(a)

(b)

(c)

(d)

Figure 22 Friction coefficient vs Load to see the repeatability of the modified crossed cylinder setup: (a) WSC, (b) DLC, (c) DLC-W, and (d) DLC-Si(O)

The behaviour of the coefficient of friction, for different load in relation to sliding distance for WSC coating obtained using the modified crossed cylinder test is shown in figure 23. Moreover, from the results presented in Tables 4 and 5, it was observed that for all coatings except DLC-Si(O), the coefficient of friction decreases with the increase in the applied load, regardless of their hardness value. This trend of self-lubricating coatings can be explained by

their typical behavior that develops a self-adaptation process. These coatings undergo a modification of their microstructure in the region of contact when subjected to high contact stress value or high temperature (see figure 24). However, there was not any relevant explanation found during the experiment which could explain the behavior of DLC-Si(O).
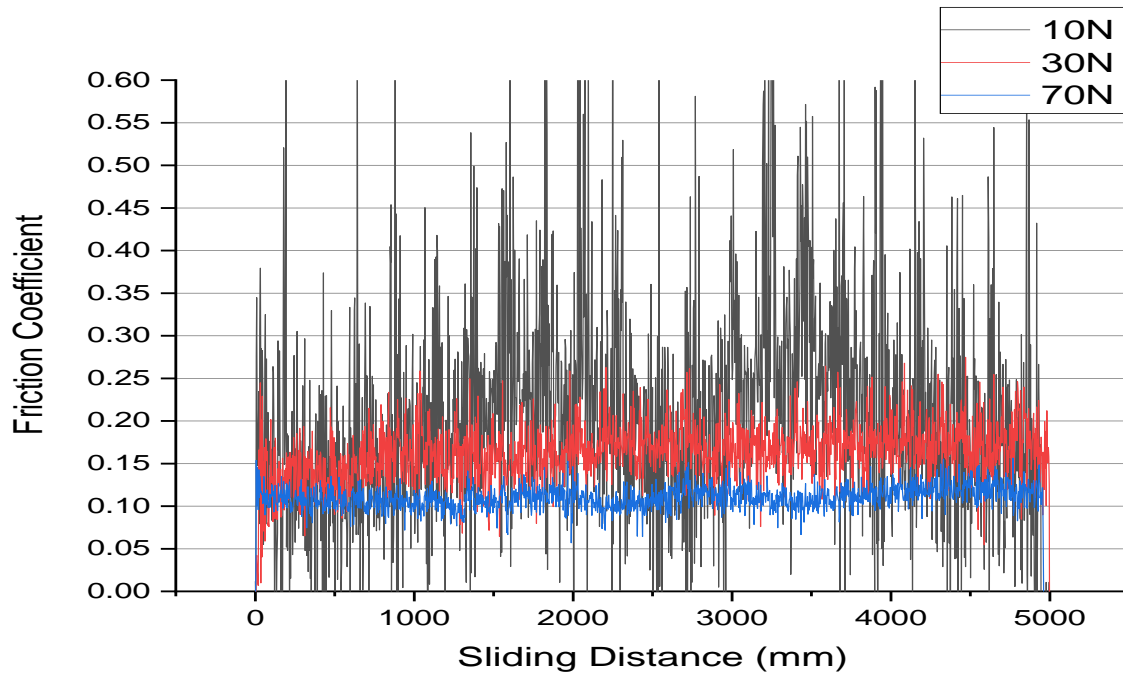

Figure 23 Effect of normal load on the friction coefficient (WSC coating)

Table 5 Results obtained from the modified crossed cylinder test

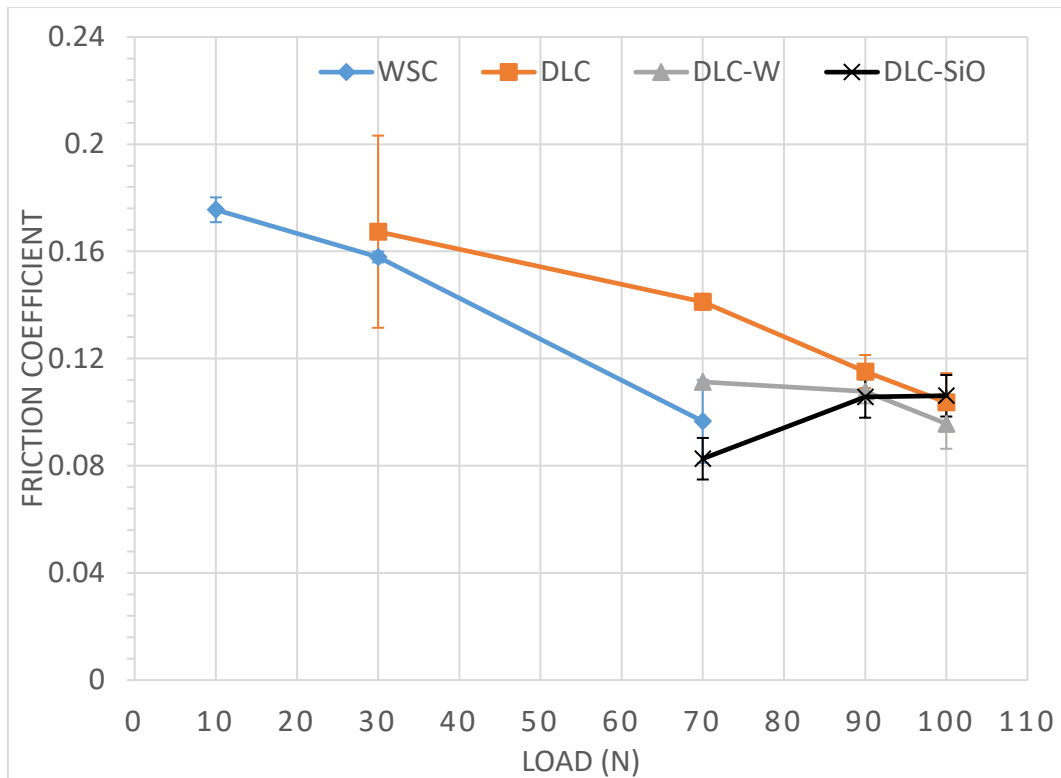| Coating	Friction coefficient for different load				
	10N	**30N**	**70N**	**90N**	**100N**
WSC	0.176	0.158	0.097		
DLC		0.167	0.141	0.115	0.104
DLC-W			0.111	0.108	0.096
DLC-SiO			0.083	0.106	0.106

Figure 24 Variation of friction coefficient with load without lubrication

Table 4 and figure 25 show that the coatings with lower hardness values tend to have severe wear. Also, it was observed that the area of the wear crater increases with the increase of the load for all the coatings. An optical microscope was used to measure the wear area of the crater for each test. The area of the crater was calculated, considering the elliptical shape as seen in figure 26.
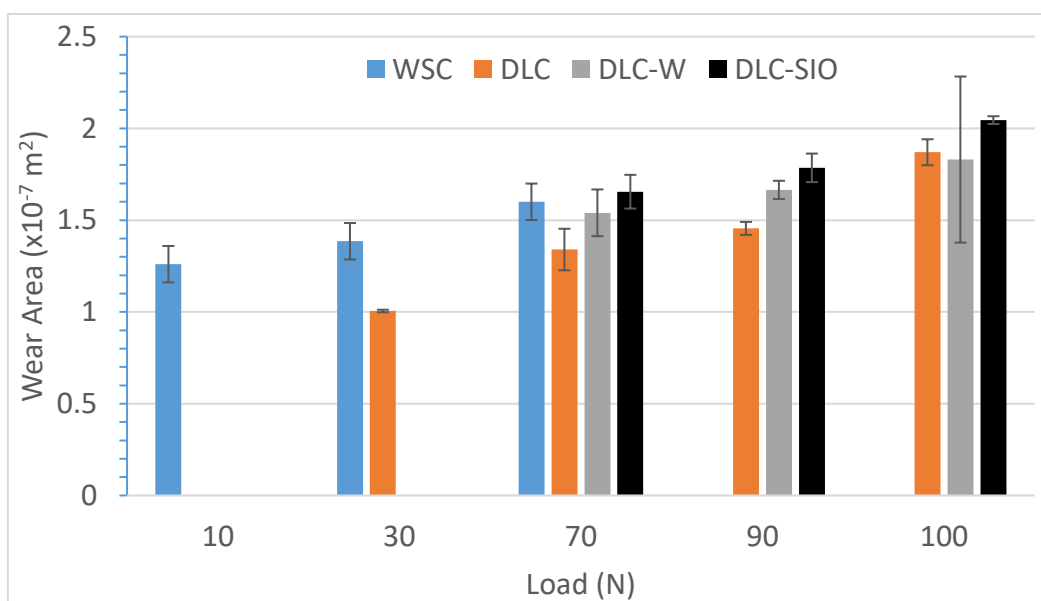

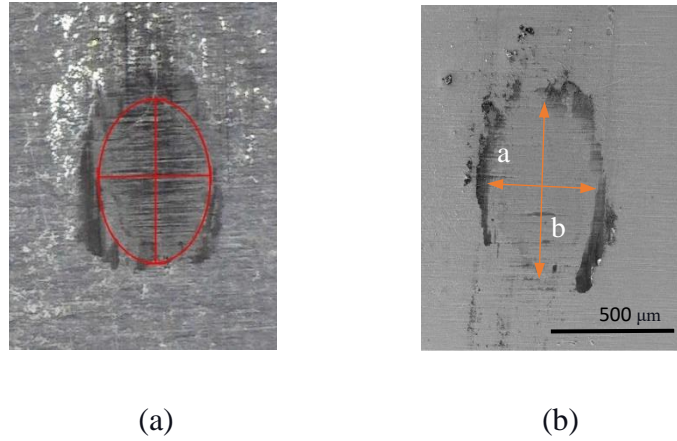*Figure 25 Variation of the wear area with the load applied*

(a)   (b)

Figure 26 Wear observed in DLC-W for 100 N load (a) Under an optical microscope (100×), (b) Using SEM

The wear area for WSC coating increased from $1.26\text{x}10^{-7}$ m^2 to $1.6\text{x}10^{-7}$ m^2 with an increased load from 10N to 70N. Furthermore, WSC almost showed the lowest friction coefficient (~0.097) among all for the test carried out with the sliding distance of 5000 mm. The reason behind the low COF might be the formation of WS$_2$ rich tribofilms, in addition to chromium oxides. The electron microscopy results with EDS and color mapping show that the Cr interlayer was reached, forming chromium oxide with some adhesion of iron on the surface of coating from the counter cylinder (figure 27 and 28). According to the crystal-chemical approach, the lubricious character of oxides increases with the increase of ionic potentials [57].
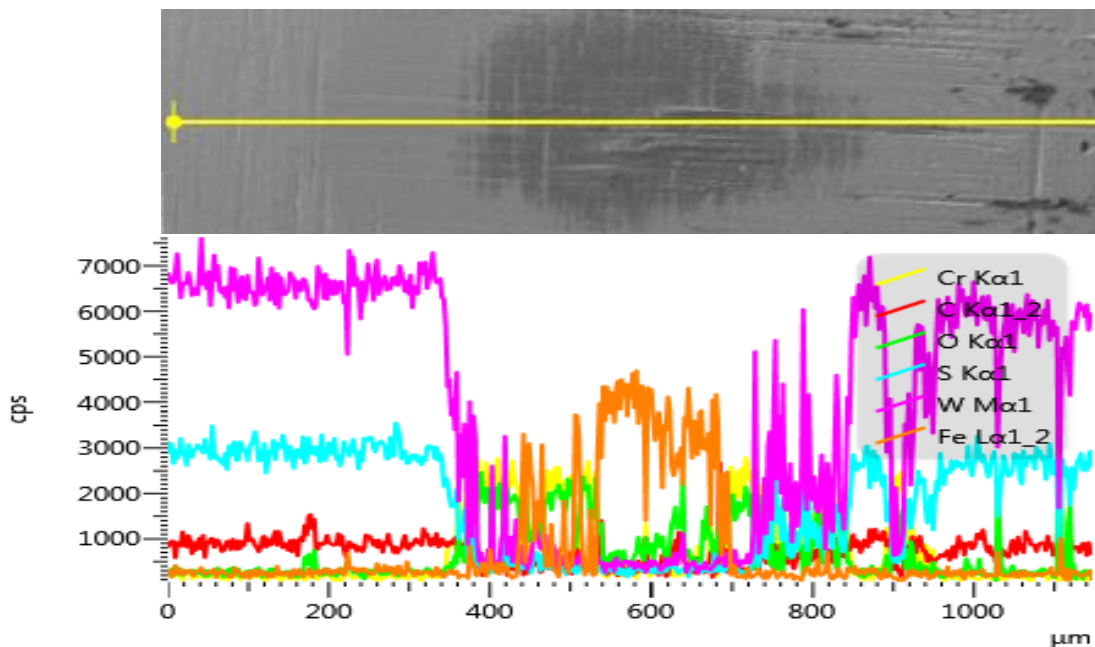

Figure 27 Chemical composition in the worn area of WSC coated cylinder, for an applied load of 70N
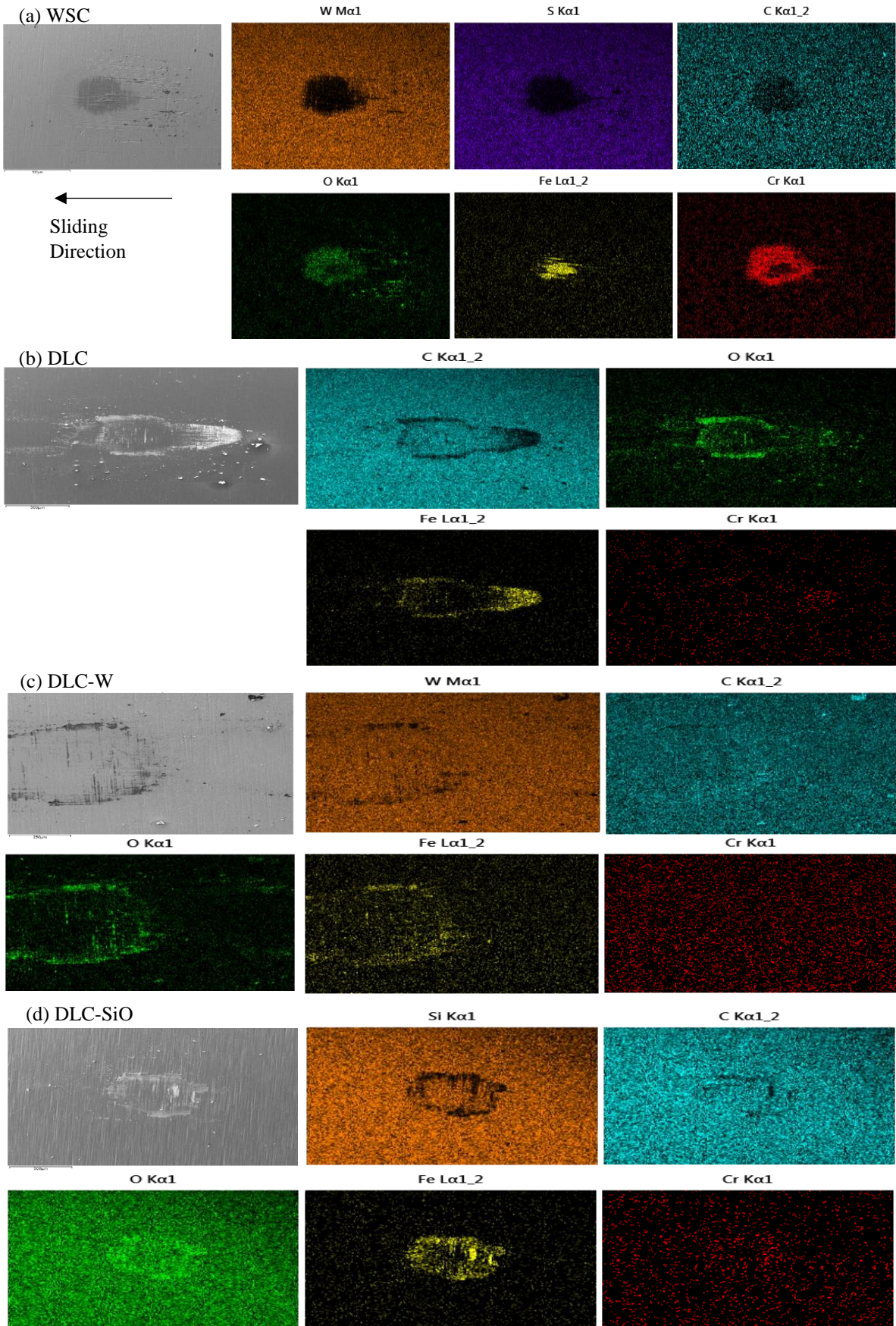
Figure 28 EDS mapping showing the occurrence of the different elements in the contact track on the coated tool for an applied load of 70N (a) WSC, (b) DLC, (c) DLC-W, and (d) DLC-Si(O)

As discussed earlier, from figure 25, the wear area for all coatings increased with the increase in load. However, DLC modified its wear behavior when the load was increased from 90N to 100N. There was a sudden increase of wear area from 1.46×10^{-7} m^2 to 1.87×10^{-7} m^2; this might have happened due to modification in its microstructure (graphitization), reducing the hardness of coating in the contact region. As observed from Figures 24 and 25, DLC-W coating maintained friction coefficient and wear profile behavior with increased load. Moreover, the color mapping and results of electron microscopy with EDS clearly show the presence of iron oxide on the wear region of all the coatings, suggesting that there is also some influence of counter body material in the contact region, as seen in Figure 27, 28 and 29.
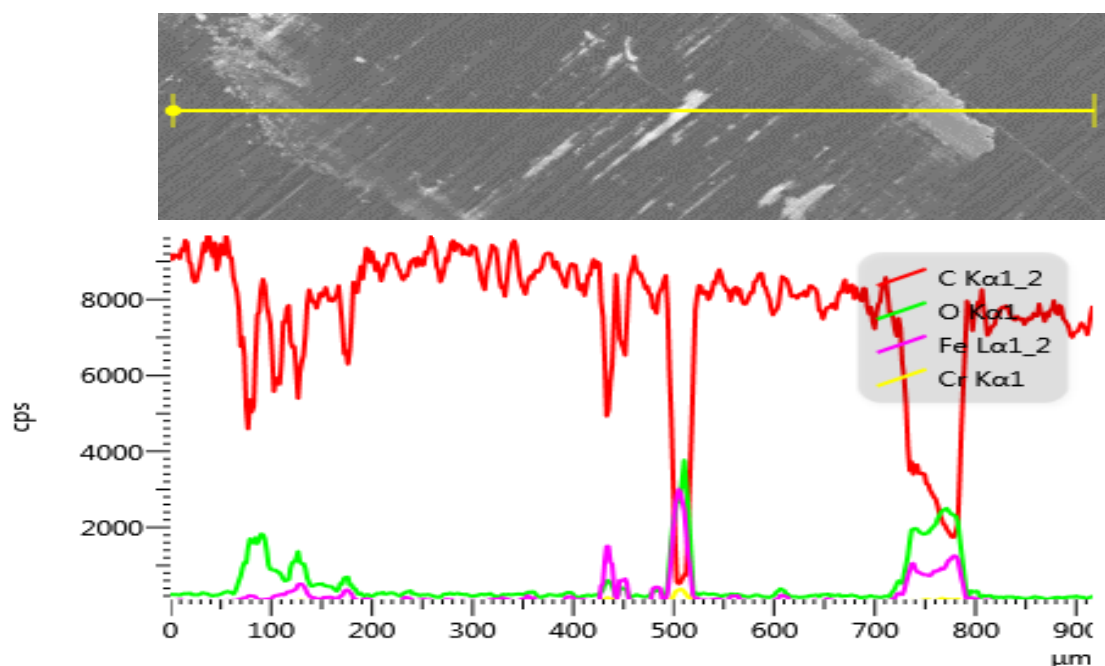

Figure 29 Chemical composition in the worn area of DLC coated cylinder, for an applied load of 100N

Though the addition of elements in the pure DLC coatings exhibits better performance as observed in previous research (literature review), an insignificant difference is observed in the result obtained using the modified crossed cylinder friction test. Despite increasing the load to a maximum contact pressure of ~1 GPa, the COF for all DLC systems was almost the same. Perhaps the energy accumulated on the wear surface of the coating was not sufficient to disturb the nanostructures formed by the additional elements. To test this theory, we tried to increase the load beyond the maximum contact pressure of ~1 GPa, but it was not possible due to the limitation of the holder and air supply system. Therefore, we varied the sliding distance of the test as 5000, 10000, and 15000 mm, thus increasing the test time. All the test parameters were

kept the same; however, the load was set to 70N. DLC-W followed both the friction and wear behavior for this test system, so it was chosen for the next tests.

From Figure 30, it is observed that with the increase of sliding distance for the DLC-W coating, there was a notable reduction in friction coefficient from ~0.12 to ~0.06. It was also observed that the coefficient of friction gradually decreased down to the sliding distance of 10000 mm and remained steady after that, thus resulting in a stable friction coefficient. This decrease in coefficient of friction is due to the self-lubricating behavior of the coating, where it forms a self-lubricating tribo layer.
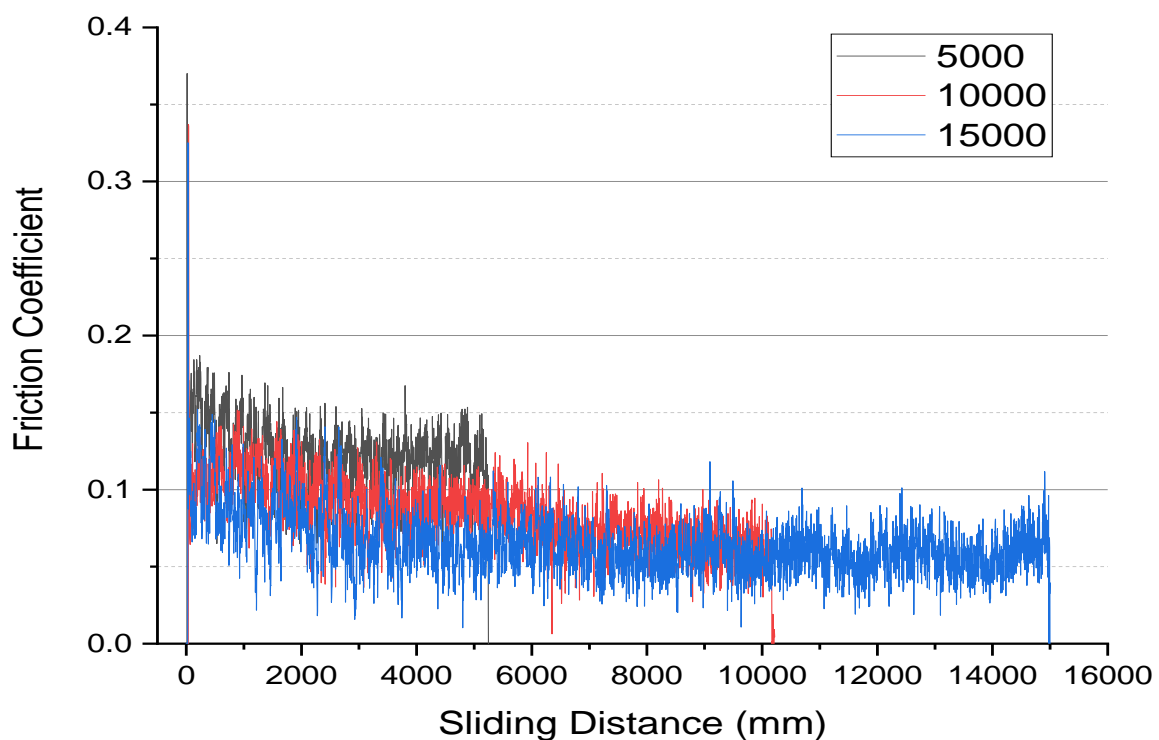
Figure 30 Variation of friction coefficient with the sliding distance; DLC-W with 70N load

Moreover, with the increase in the sliding distance from 5000 mm to 15000 mm, the wear crater area in the coating increased from $1.56\text{x}10^{-7}$ m^2 to $2.13\text{x}10^{-7}$ m^2 (see figure 31). The color mapping and results of electron microscopy with EDS clearly show iron oxide's presence on the wear region of the coatings without reaching the chromium interlayer (see Figures 32 and 33).
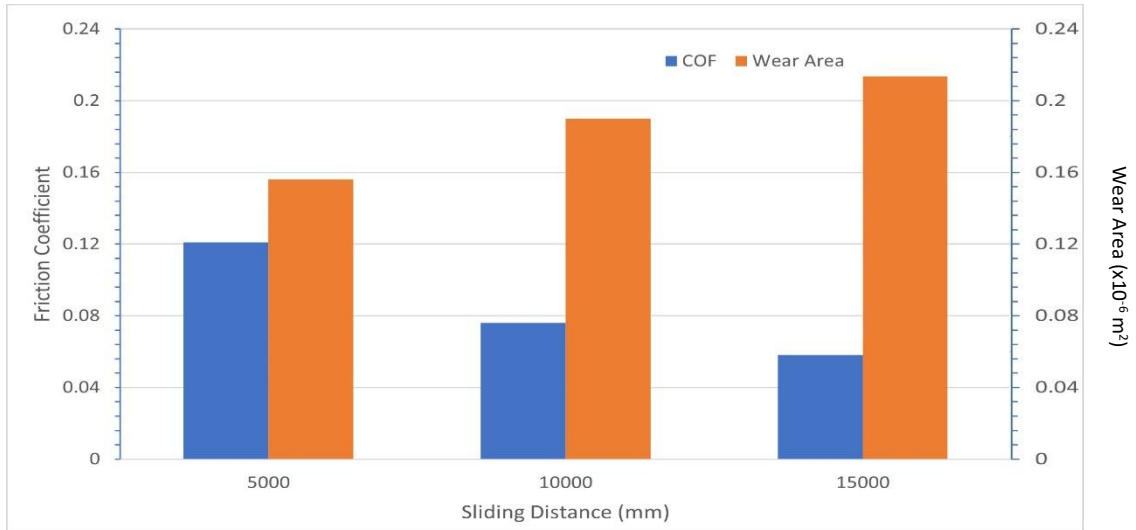
Figure 31 Wear area on DLC-W coating and friction coefficient for the DLC-W/steel pair. Load, 70N with varying sliding distance

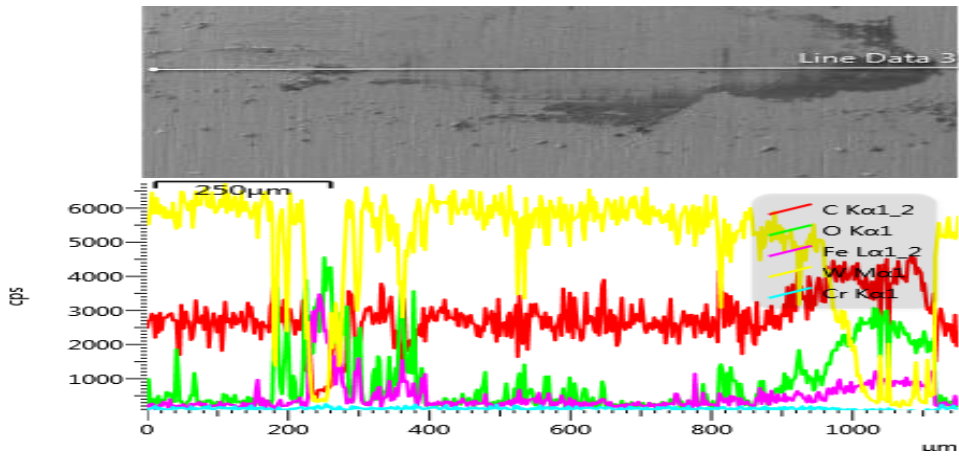*Figure 32 Chemical composition in the worn area of DLC-W coated cylinder, for an applied load of 70N and sliding distance of 15000mm*
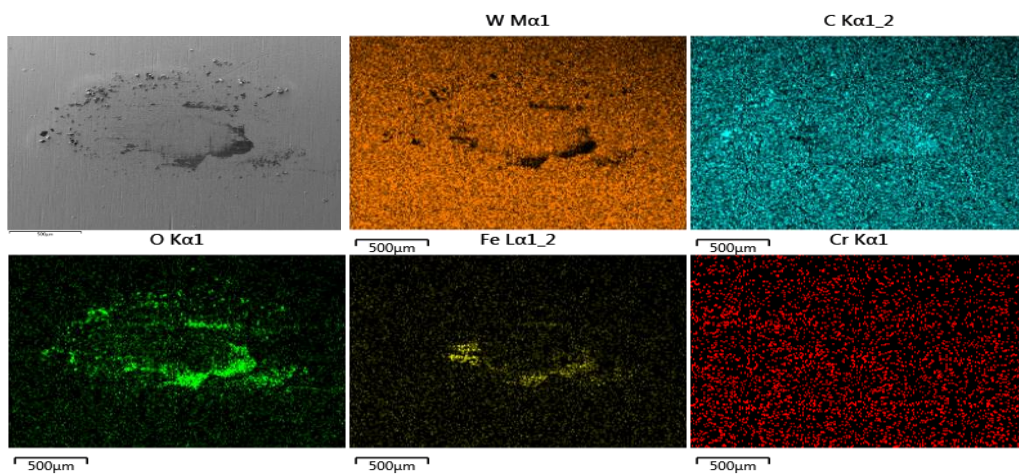
Figure 33 EDS mapping showing the occurrence of the different elements in the contact track on the DLC-W coated tool for an applied load of 70N and sliding distance of 15000mm

Raman spectra were obtained for DLC-W coating with the test condition (70N load and 15000 mm sliding distance) at three different locations, i.e., coated surface (as deposited), debri, and center of the wear track (see figure 34 and 35). D (defect region) and G (graphitic region) carbon bands were observed at 1385 cm^{-1} and 1565 cm^{-1}, respectively, in the case of debri and coated surface (as deposited). However, the Raman spectrum of the center of wear scar observed that the G band moved to 1600 cm^{-1} from 1565 cm^{-1} indicating graphitization during the wear test. Additionally, I(D)/I(G) ratio is also increased, suggesting graphitization [58].

Figure 34 Locations used for Raman Spectroscopy (DLC-W_70N_15000mm)

Figure 35 Raman Spectra at different points for DLC-W_70N_15000mm

8. Conclusion

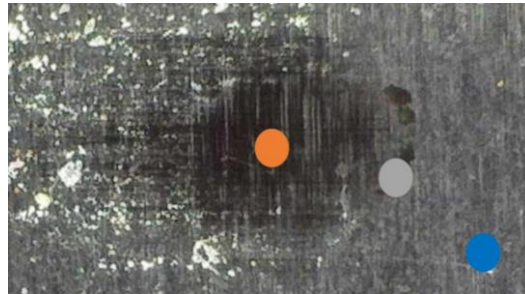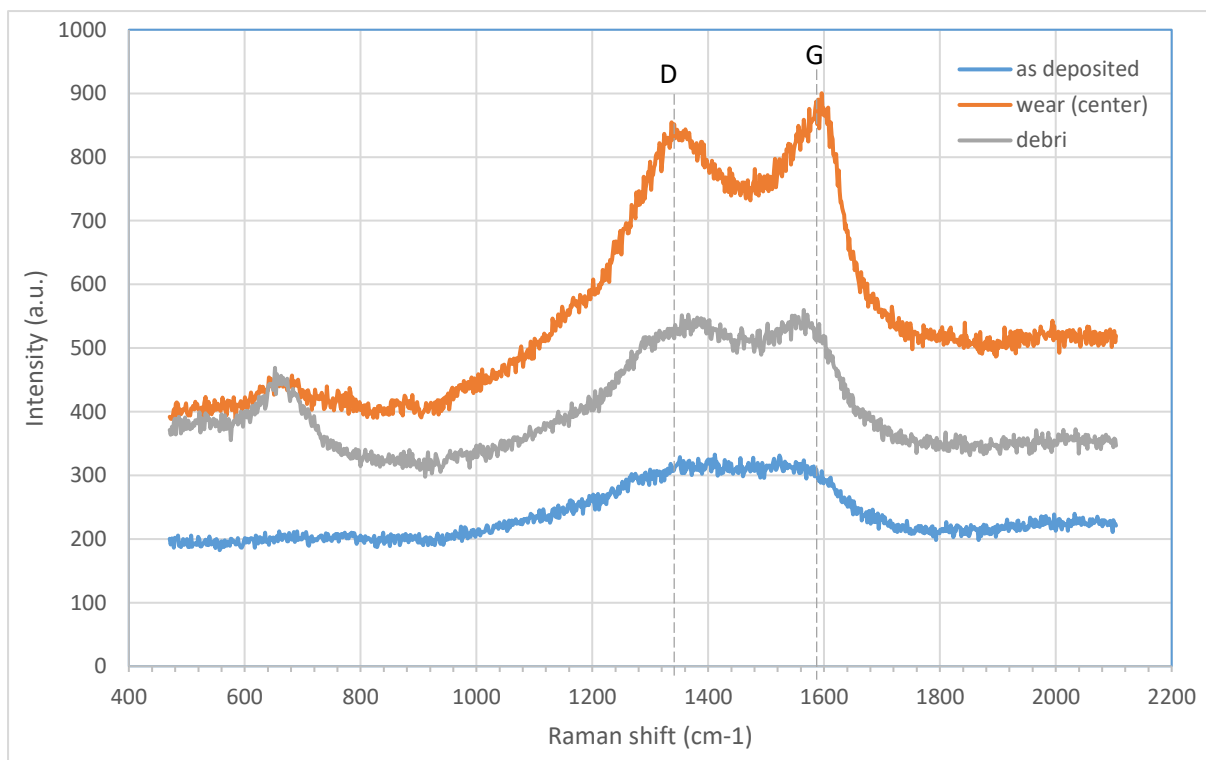It was observed that with the increase in load, the friction coefficient decreases for all the coatings except DLC-Si(O), while the wear area for all the coatings increases with the increase in load. For the tests carried out with the sliding distance of 5000 mm, WSC almost presented the lowest COF among all, which might have resulted due to the formation of WS_2 rich tribofilms, in addition to chromium oxides. For DLC coatings, the presence of additional elements in the microstructure can cause a reduction in the internal stresses of the coating without compromising its tribological performance. The chromium interlayer was not reached for any of the DLC coatings, representing a good commitment of friction coefficient to mass wear for high loads. When the test duration was increased to three times the initial test time, the coefficient of friction decreased by 52% against an increase of 36% in wear area for DLC-W coating tested in dry lubrication and room temperature. A relevant explanation was not found for the behavior of DLC-Si(O) resulted in this test system, which should be further explored in the future.

With all the results and their analysis, the potential of the modified crossed cylinder technique for a friction test to replicate service conditions occurring in the process of actual cutting/forming operation was demonstrated. Similar to other testing methods, the results of this friction test for self-lubricating coating should be accompanied by the chemical-structural analysis of the worn surfaces. To support the conclusions achieved in the last part of this study, additional tests for all coatings with the increased test duration should be performed. Moreover, to better analyze the tribological behavior, Raman spectroscopy should be carried out for the (micro)structural analysis of the wear area. It should be noted that while repeating the test for a longer test duration, the counter cylinder should be polished several times, which might affect its microstructure. Then, small variations in the contact region of the coating and counter body can be expected, which may influence the final tribological values.

9. References

[1] B. Bhushan and B. K. Gupta, "Handbook of tribology: materials, coatings, and surface treatments," 1991.

[2] B. Bhushan, *Tribology and mechanics of magnetic storage devices*. Springer Science & Business Media, 2012.

[3] T. Sato, Y. Tada, M. Ozaki, K. Hoke, and T. Besshi, "A crossed-cylinders testing for evaluation of wear and tribological properties of coated tools," *Wear*, vol. 178, no. 1–2, pp. 95–100, 1994.

[4] B. Zhu, G. L. Kelly, and J. Mardel, "An investigation of tribological properties of CN and TiCN coatings," *J. Mater. Eng. Perform.*, vol. 13, no. 4, pp. 481–487, 2004.

[5] J. Gerth, J. Heinrichs, H. Nyberg, M. Larsson, and U. Wiklund, "Evaluation of an intermittent sliding test for reproducing work material transfer in milling operations," *Tribol. Int.*, vol. 52, pp. 153–160, 2012.

[6] J. Heinrichs, M. Olsson, and S. Jacobson, "Initial deformation and wear of cemented carbides in rock drilling as examined by a sliding wear test," *Int. J. Refract. Met. Hard Mater.*, vol. 64, pp. 7–13, 2017.

[7] D. A. Hanaor, Y. Gan, and I. Einav, "Static friction at fractal interfaces," *Tribol. Int.*, vol. 93, pp. 229–238, 2016.

[8] "How to reduce the effects of stick-slip (stiction) in linear guides," *Linear Motion Tips*, Mar. 13, 2020. https://www.linearmotiontips.com/how-to-reduce-the-effects-of-stiction-stick-slip-in-linear-guides/ (accessed Jan. 20, 2021).

[9] I. M. Hutchings, "Leonardo da Vinci′s studies of friction," *Wear*, vol. 360, pp. 51–66, 2016.

[10] C.-H. Lee and A. A. Polycarpou, "Static Friction Experiments and Verification of an Improved Elastic-Plastic Model Including Roughness Effects," *J. Tribol.*, vol. 129, no. 4, pp. 754–760, Apr. 2007, doi: 10.1115/1.2768074.

[11] M. Kandeva-Ivanova, A. Vencl, and D. Karastoyanov, *Advanced tribological coatings for heavy-duty applications: case studies*, First edition. Sofia: Prof. Marin Drinov Publishing House of Bulgarian Academy of Sciences, 2016.

[12] M. J. Neale, *Lubrication and reliability handbook*. Newnes, 2001.

[13] L. Shan, Y. Wang, J. Li, X. Jiang, and J. Chen, "Improving tribological performance of CrN coatings in seawater by structure design," *Tribol. Int.*, vol. 82, pp. 78–88, 2015.

[14] N. Sharma, S. N. Alam, B. C. Ray, S. Yadav, and K. Biswas, "Wear behavior of silica and alumina-based nanocomposites reinforced with multi walled carbon nanotubes and graphene nanoplatelets," *Wear*, vol. 418, pp. 290–304, 2019.

[15] D. E. T. Shepherd and K. D. Dearn, "Wear processes in polymer implants," in *Durability and Reliability of Medical Polymers*, Elsevier, 2012, pp. 143–163.

[16] G. W. Stachowiak, *Wear: materials, mechanisms and practice*. John Wiley & Sons, 2006.

[17] B. Bhushan, *Principles and applications of tribology*. John Wiley & Sons, 1999.

[18] W. Barrois, "Repeated plastic deformation as a cause of mechanical surface damage in fatigue, wear, fretting-fatigue, and rolling fatigue: A review," *Int. J. Fatigue*, vol. 1, no. 4, pp. 167–189, 1979.

[19] B. Bhushan, *Modern tribology handbook. 1. Principles of tribology*. CRC press, 2001.

[20] T. Nicholas, "Critical issues in high cycle fatigue," *Int. J. Fatigue*, vol. 21, pp. S221–S231, 1999.

[21] H. A. Padilla and B. L. Boyce, "A review of fatigue behavior in nanocrystalline metals," *Exp. Mech.*, vol. 50, no. 1, pp. 5–23, 2010.

[22] M. D. Sangid, "The physics of fatigue crack initiation," *Int. J. Fatigue*, vol. 57, pp. 58–72, 2013.

[23] K. Hokkirigawa and K. Kato, "An experimental and theoretical investigation of ploughing, cutting and wedge formation during abrasive wear," *Tribol. Int.*, vol. 21, no. 1, pp. 51–57, 1988.

[24] L. Lawson, E. Y. Chen, and M. Meshii, "Near-threshold fatigue: a review," *Int. J. Fatigue*, vol. 21, pp. S15–S34, 1999.

[25] H. Mughrabi, "Microstructural fatigue mechanisms: Cyclic slip irreversibility, crack initiation, non-linear elastic damage analysis," *Int. J. Fatigue*, vol. 57, pp. 2–8, 2013.

[26] K. Holmberg and A. Matthews, *Coatings tribology: properties, mechanisms, techniques and applications in surface engineering*. Elsevier, 2009.

[27] J. Takadoum, "Materials and Surface Engineering in Tribology. ISTE Ltd. and John Wiley & Sons," *Inc Lond. Hoboken*, pp. 66–71, 2008.

[28] H. Czichos and K.-H. Habig, *Tribologie-Handbuch: Tribometrie, Tribomaterialien, Tribotechnik*. Springer-Verlag, 2010.

[29] E. D. Braun, "Methods and Devices for Tribotechnical Tests," *KV Frolov Mosc. URSS*, pp. 367–414, 2007.

[30] E. Santner, *Reibung und Verschleiß von Werkstoffen, Bauteilen und Konstruktionen: tribologische Optimierung und Schadensbekämpfung*. expert-Verlag, 2004.

[31] D. Li and P. LEROUX, "BLOCK-ON-RING SLIDING WEAR EVALUATION," Technical Report, 2016.

[32] B. Podgornik, S. Hogmark, and J. Pezdirnik, "Comparison between different test methods for evaluation of galling properties of surface engineered tool surfaces," *Wear*, vol. 257, no. 7–8, pp. 843–851, 2004.

[33] R. J. K. Wood *et al.*, "Electrostatic monitoring of the effects of carbon black on lubricated steel/steel sliding contacts," in *Tribology and Interface Engineering Series*, vol. 48, Elsevier, 2005, pp. 109–121.

[34] P. J. Blau and K. G. Budinski, "Development and use of ASTM standards for wear testing," *Wear*, vol. 225, pp. 1159–1170, 1999.

[35] T. Aiso and U. Wiklund, "Influence of contact parameters on material transfer from steel to TiN coated tool–optimisation of a sliding test for simulation of material transfer in milling," *Tribol.-Mater. Surf. Interfaces*, vol. 10, no. 3, pp. 107–116, 2016.

[36] P. Olander and J. Heinrichs, "Initiation and propagation of tool wear in turning of titanium alloys–Evaluated in successive sliding wear test," *Wear*, vol. 426, pp. 1658–1666, 2019.

[37] B. Gupta and B. Bhushan, "Handbook of Tribology," 1997.

[38] S. Hogmark, S. Jacobson, and M. Larsson, "Design and evaluation of tribological coatings," *Wear*, vol. 246, no. 1–2, pp. 20–33, 2000.

[39] G. S. Goindi and P. Sarkar, "Dry machining: a step towards sustainable machining–challenges and future directions," *J. Clean. Prod.*, vol. 165, pp. 1557–1571, 2017.

[40] Y. Lian, J. Deng, S. Li, G. Yan, and S. Lei, "Friction and wear behavior of WS 2/Zr self-lubricating soft coatings in dry sliding against 40Cr-hardened steel balls," *Tribol. Lett.*, vol. 53, no. 1, pp. 237–246, 2014.

[41] N. Renevier, N. Lobiondo, V. Fox, D. Teer, and J. Hampshire, "Performance of MoS2/metal composite coatings used for dry machining and other industrial applications," *Surf. Coat. Technol.*, vol. 123, no. 1, pp. 84–91, 2000.

[42] K. Zhang, J. Deng, Z. Ding, X. Guo, and L. Sun, "Improving dry machining performance of TiAlN hard-coated tools through combined technology of femtosecond laser-textures and WS2 soft-coatings," *J. Manuf. Process.*, vol. 30, pp. 492–501, 2017.

[43] T. Polcar, M. Evaristo, and A. Cavaleiro, "Friction of Self-Lubricating W-S-C Sputtered Coatings Sliding Under Increasing Load," *Plasma Process. Polym.*, vol. 4, no. S1, pp. S541–S546, 2007.

[44] T. Vuchkov, M. Evaristo, T. bin Yaqub, T. Polcar, and A. Cavaleiro, "Synthesis, microstructure and mechanical properties of W–S–C self-lubricant thin films deposited by magnetron sputtering," *Tribol. Int.*, p. 106363, 2020.

[45] M. Evaristo, T. Polcar, and A. Cavaleiro, "Tribological behaviour of W-alloyed carbon-based coatings in dry and lubricated sliding contact," *Lubr. Sci.*, vol. 26, no. 6, pp. 428–439, 2014.

[46] M. Evaristo, F. Fernandes, and A. Cavaleiro, "Room and high temperature tribological behaviour of W-DLC coatings produced by DCMS and hybrid DCMS-HiPIMS configuration," *Coatings*, vol. 10, no. 4, p. 319, 2020.

[47] R. O. Dillon, J. A. Woollam, and V. Katkanant, "Use of Raman scattering to investigate disorder and crystallite formation in as-deposited and annealed carbon films," *Phys. Rev. B*, vol. 29, no. 6, p. 3482, 1984.

[48] J. C. Damasceno, S. S. Camargo Jr, F. L. Freire Jr, and R. Carius, "Deposition of Si-DLC films with high hardness, low stress and high deposition rates," *Surf. Coat. Technol.*, vol. 133, pp. 247–252, 2000.

[49] W. J. Yang, T. Sekino, K. B. Shim, K. Niihara, and K. H. Auh, "Microstructure and tribological properties of SiOx/DLC films grown by PECVD," *Surf. Coat. Technol.*, vol. 194, no. 1, pp. 128–135, 2005.

[50] J. Choi, S. Nakao, S. Miyagawa, M. Ikeyama, and Y. Miyagawa, "The effects of Si incorporation on the thermal and tribological properties of DLC films deposited by PBII&D with bipolar pulses," *Surf. Coat. Technol.*, vol. 201, no. 19–20, pp. 8357–8361, 2007.

[51] C. Venkatraman, C. Brodbeck, and R. Lei, "Tribological properties of diamond-like nanocomposite coatings at high temperatures," *Surf. Coat. Technol.*, vol. 115, no. 2–3, pp. 215–221, 1999.

[52] M. Evaristo, R. Azevedo, C. Palacio, and A. Cavaleiro, "Influence of the silicon and oxygen content on the properties of non-hydrogenated amorphous carbon coatings," *Diam. Relat. Mater.*, vol. 70, pp. 201–210, 2016.

[53] V. P. Astakhov, "Tribology of metal cutting," 2006.

[54] E. M. Trent and P. K. Wright, *Metal cutting*. Butterworth-Heinemann, 2000.

[55] P. Hedenqvist, M. Olsson, and S. Söderberg, "Influence of TiN coating on wear of high speed steel tools as studied by new laboratory wear test," *Surf. Eng.*, vol. 5, no. 2, pp. 141–150, 1989.

[56] T. Vuchkov, M. Evaristo, T. B. Yaqub, and A. Cavaleiro, "The effect of substrate location on the composition, microstructure and mechano-tribological properties of WSC coatings deposited by magnetron sputtering," *Surf. Coat. Technol.*, vol. 386, p. 125481, 2020.

[57] A. Öztürk, K. Ezirmik, K. Kazmanlı, M. Ürgen, O. Eryılmaz, and A. Erdemir, "Comparative tribological behaviors of TiN, CrN and MoNCu nanocomposite coatings," *Tribol. Int.*, vol. 41, no. 1, pp. 49–59, 2008.

[58] A. C. Ferrari and J. Robertson, "Interpretation of Raman spectra of disordered and amorphous carbon," *Phys. Rev. B*, vol. 61, no. 20, p. 14095, 2000.